Loss of *Biglycan* Enhances Thrombin Generation in *Apolipoprotein E*-Deficient Mice

Implications for Inflammation and Atherosclerosis

Maria Grandoch, Christina Kohlmorgen, Ariane Melchior-Becker, Kathrin Feldmann, Susanne Homann, Julia Müller, Lena-Sophia Kiene, Jinyang Zeng-Brouwers, Friederike Schmitz, Nadine Nagy, Amin Polzin, Nina S. Gowert, Margitta Elvers, Philipp Skroblin, Xiaoke Yin, Manuel Mayr, Liliana Schaefer, Lisa R. Tannock, Jens W. Fischer

Objective—Thrombin signaling promotes atherosclerosis by initiating inflammatory events indirectly through platelet activation and directly via protease-activated receptors. Therefore, endogenous thrombin inhibitors may be relevant modulators of atheroprogression and cardiovascular risk. In addition, endogenous thrombin inhibitors may affect the response to non–vitamin K-dependent oral anticoagulants. Here, the question was addressed whether the small leucine-rich proteoglycan biglycan acts as an endogenous thrombin inhibitor in atherosclerosis through activation of heparin cofactor II.

Approach and Results—Biglycan concentrations were elevated in the plasma of patients with acute coronary syndrome and in male *Apolipoprotein E*-deficient (*ApoE*$^{-/-}$) mice. Biglycan was detected in the glycocalyx of capillaries and the subendothelial matrix of arterioles of *ApoE*$^{-/-}$ mice and in atherosclerotic plaques. Thereby a vascular compartment is provided that may mediate the endothelial and subendothelial activation of heparin cofactor II through biglycan. *ApoE* and *Bgn* double-deficient (*ApoE*$^{-/-}$/*Bgn*$^{-/0}$) mice showed higher activity of circulating thrombin, increased platelet activation and platelet adhesion in vivo, supporting a role of biglycan in balancing thrombin activity. Furthermore, concentrations of circulating cytokines and aortic macrophage content were elevated in *ApoE*$^{-/-}$/*Bgn*$^{-/0}$ mice, suggesting a proinflammatory phenotype. Elevated platelet activation and macrophage accumulation were reversed by treating *ApoE*$^{-/-}$/*Bgn*$^{-/0}$ mice with the thrombin inhibitor argatroban. Ultimately, *ApoE*$^{-/-}$/*Bgn*$^{-/0}$ mice developed aggravated atherosclerosis.

Conclusions—The present results indicate that biglycan plays a previously unappreciated protective role during the progression of atherosclerosis by inhibiting thrombin activity, platelet activation, and finally macrophage-mediated plaque inflammation. (***Arterioscler Thromb Vasc Biol*. 2016;36:e41-e50. DOI: 10.1161/ATVBAHA.115.306973.)**

Key Words: atherosclerosis ■ biglycan ■ blood platelets ■ inflammation ■ thrombin

Thrombin is crucially involved in clot formation and platelet activation. Furthermore, the direct cellular effects of thrombin are mediated through activation of protease-activated receptors that regulate the function of immune cells, smooth muscle cells (SMC), and endothelial cells.[1,2] Clinically, thrombin activity is targeted with heparins and heparinoids that act as direct activators of anti–thrombin III and are of critical importance to prevent and treat deep vein thrombosis. In addition, the coagulation cascade including thrombin is targeted by vitamin K antagonists such as warfarin to prevent stroke in patients with atrial fibrillation. Recently, new non–vitamin K-dependent oral anticoagulants directly inhibiting activated factors X and II have entered clinical practice to prevent deep vein thrombosis and strokes in atrial fibrillation patients, and—in case of rivaroxaban—even acute coronary syndrome.[3] In addition to regulating hemostasis and thereby affecting the rate of acute cardiovascular events, thrombin-stimulated platelets promote neutrophil and macrophage-driven inflammation.

Received on: December 2, 2015; final version accepted on: March 17, 2016.

From the Institut für Pharmakologie und Klinische Pharmakologie, Universitätsklinikum der Heinrich-Heine-Universität Düsseldorf, Düsseldorf, Germany (M.G., C.K., A.M.-B., K.F., S.H., J.M., L.-S.K., F.S., N.N., J.W.F.); Cardiovascular Research Institute Düsseldorf (CARID), Universitätsklinikum der Heinrich-Heine-Universität Düsseldorf, Düsseldorf, Germany (M.G., C.K., A.M.-B., K.F., S.H., J.M., L.-S.K., F.S., N.N., A.P., J.W.F.); Klinik für Kardiologie, Pneumologie und Angiologie, Universitätsklinikum der Heinrich-Heine-Universität Düsseldorf, Düsseldorf, Germany (A.P.); Pharmazentrum Frankfurt, Institut für Allgemeine Pharmakologie und Toxikologie/ZAFES, Klinikum der Goethe-Universität, Frankfurt am Main, Germany (J.Z.-B., L.S.); Institut für Hämostaseologie, Hämotherapie und Transfusionsmedizin, Universitätsklinikum der Heinrich-Heine-Universität Düsseldorf, Düsseldorf, Germany (N.S.G., M.E.); King's British Heart Foundation Centre, King's College London, London, United Kingdom (P.S., X.Y., M.M.); and Division of Endocrinology and Molecular Medicine, Saha Cardiovascular Research Center, University of Kentucky, Lexington (L.R.T.).

The online-only Data Supplement is available with this article at http://atvb.ahajournals.org/lookup/suppl/doi:10.1161/ATVBAHA.115.306973/-/DC1.

Correspondence to Jens W. Fischer, PhD, Institut für Pharmakologie und Klinische Pharmakologie, Universitätsklinikum der Heinrich-Heine-Universität Düsseldorf, Moorenstr. 5, 40225 Düsseldorf, Germany. E-mail jens.fischer@uni-duesseldorf.de

Nonstandard Abbreviations and Acronyms	
ACS	acute coronary syndrome
DS	dermatan sulfate
ETP	endogenous thrombin potential
HCII	heparin cofactor II
IL	interleukin
SMC	smooth muscle cells

The former by platelet–neutrophil complexes[4] and the latter by release of proinflammatory mediators from thrombin-activated platelets.[5] Thereby, thrombin represents a central factor in both the pathogenesis of atherosclerosis and the occurrence of acute thrombotic events.

First, endogenous modulators of thrombin activity may indirectly contribute to the cardiovascular risk and the event rates.[6,7] Therefore, given the critical importance of thrombin activity in cardiovascular disease, endogenous mechanisms controlling thrombin activity are of great importance. Second, it may be hypothesized that the extent of endogenous thrombin inhibition also affects the therapeutic efficiency of non–vitamin K-dependent oral anticoagulants. Two important endogenous thrombin inhibitors are known: antithrombin III activated by heparin and heparin cofactor II (HCII) activated by dermatan sulfate (DS). HCII is generally activated by chondroitin sulfate B (DS) and, in part, also by chondroitin sulfate, which are attached to the core proteins of a variety of proteoglycans such as versican and biglycan. Biglycan contains 2 N-terminal DS side chains and has indeed been shown to activate HCII.[8]

It is to date unclear where biglycan is localized to fulfill its function to activate HCII and whether the localization is subject to regulation during atherosclerosis. Biglycan is in general synthesized by endothelial cells, SMCs, fibroblasts, and macrophages.[9–11] Accordingly, vascular biglycan deposition occurs in the neointima and the adventitia of arterial blood vessels. In line with a critical function of biglycan in the neointimal plaque matrix and hemostasis, biglycan was found to be absent from the luminal layer of thrombosed-eroded plaques.[12] Therefore, the absence of biglycan from the plaque surface might promote atherothrombosis.[12] In addition, endothelial cells express large amounts of biglycan and circulating biglycan has been detected in the plasma. Therefore, with respect to atherosclerosis, it is of interest whether biglycan is present in the glycocalyx and the subendothelial matrix and whether the amount of circulating biglycan is altered during atheroprogression. Furthermore, it is to date unknown whether biglycan as an endogenous thrombin inhibitor also ameliorates thrombin-driven inflammation during atheroprogression.

Another aspect of the biological function of biglycan is to contribute to the stability of the fibrous cap in accordance with the known function of biglycan in collagen fibrillogenesis.[13] However, the aforementioned potentially antiatherosclerotic functions of biglycan are opposed by published findings demonstrating that soluble biglycan promotes inflammation in acute highly inflammatory diseases such as sepsis and non-infectious renal injury[14,15] and that it contributes to vascular lipid retention.[16,17]

All considered, the effect of biglycan on atherosclerosis in vivo and its underlying mechanisms can hardly be predicted because biglycan modulates both anti- and proatherosclerotic mechanisms. Therefore, the aim of this study was to determine the vascular compartmentalization of biglycan in a mouse model of atherosclerosis and to unravel the overall effect of biglycan on thrombin activity, inflammation, and atheroprogression using mice double-deficient in *Apolipoprotein E* and *Bgn* (*ApoE*$^{-/-}$/*Bgn*$^{-/0}$ mice). This study seems to be of translational interest because the extent of endogenous thrombin inhibition by biglycan/HCII may affect the response to pharmacological thrombin/Xa inhibitors and may contribute to the cardiovascular risk.

Materials and Methods

Materials and Methods are available in the online-only Data Supplement.

Results

General Characteristics of *ApoE*$^{-/-}$/*Bgn*$^{-/0}$ Mice

Basic characterization of *ApoE*$^{-/-}$ and *ApoE*$^{-/-}$/*Bgn*$^{-/0}$ mice detected no differences between genotypes with respect to heart rate, diastolic and systolic blood pressure, total body fat, and plasma concentrations of total cholesterol, low-density lipoprotein, very-low-density lipoprotein, high-density lipoprotein, and insulin (Figure I in the online-only Data Supplement). In addition, physical activity, food intake, mean O_2 consumption, and mean CO_2 production were unchanged (Figure II in the online-only Data Supplement).

Biglycan Circulates in Human and Murine Plasma and Localizes to the Wall of Small Blood Vessels in *ApoE*-Deficient Mice

DS (also called chondroitin sulfate B) is known to activate HCII, thereby inhibiting thrombin activity in a similar manner as the activated heparin–antithrombin III complex. Two DS side chains are attached to the N terminus of biglycan. In this study, it is considered that gagylated biglycan might serve as an inhibitor of thrombin activity in *ApoE*-deficient mice. In atherosclerosis, expression of biglycan has been demonstrated in atherosclerotic plaques[12,18] where it may confer local inhibition of thrombin. Here, it was investigated whether biglycan (1) circulates, (2) is present in the glycocalyx, and (3) is deposited in the subendothelial matrix. In line with these assumptions, it was observed that biglycan circulates in human plasma and was even higher in the plasma of patients with acute coronary syndrome (Figure 1A and 1B) when compared with patients without coronary heart disease. Importantly, patient groups did not differ with regard to basal clinical characteristics, risk factors and medication (Table I in the online-only Data Supplement). Similarly, biglycan was detectable in plasma of C57BL/6J wild-type controls and was increased in the plasma of atherosclerotic *ApoE*$^{-/-}$ mice (Figure 1C and 1D). The vascular staining of biglycan showed a difference in biglycan localization between capillaries and arterioles. Capillaries were defined by isolectin B4-positive cells forming lumina ≤10 μm. Biglycan was clearly detectable on the luminal surface of capillary endothelial cells (Figure 1E) using fluorescence

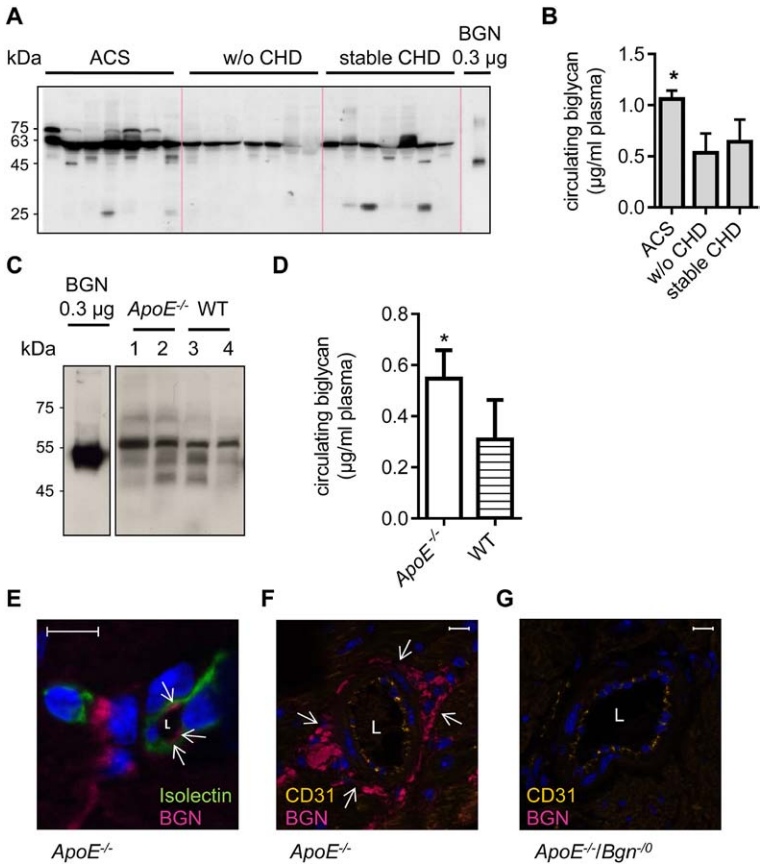

Figure 1. Biglycan (BGN) circulates and is present in the glycocalyx and subendothelial matrix. **A** and **B**, Increased amounts of circulating BGN in human plasma samples of patients with acute coronary syndrome (ACS) compared with patients without coronary heart disease (w/o CHD) and with stable CHD. **A**, Western blot of BGN core protein after chondroitinase ABC digestion from human plasma samples and (**B**) the respective quantification; n=7. **C**, Western blot of circulating BGN from murine plasma samples from *Apolipoprotein E*-deficient (*ApoE*$^{-/-}$) and C57BL/6 wild-type (WT) mice and (**D**) respective quantification; n=5. Recombinant BGN (0.3 µg), digested with chondroitinase ABC, is shown as a standard. **E**–**G**, Immunohistochemical analysis of BGN in cardiac tissue from *ApoE*$^{-/-}$ and *ApoE*$^{-/-}$/*Bgn*$^{-/0}$ mice. Representative staining of (**E**) BGN (magenta) and endothelial cells (isolectin, green) in capillaries (**F** and **G**) BGN (magenta) and endothelial cells (CD31, orange) in arterioles of *ApoE*$^{-/-}$mice. **G**, Absence of BGN in vessels of *ApoE*$^{-/-}$/*Bgn*$^{-/0}$ mice. Nuclear counterstaining was performed with DAPI (4',6-diamidino-2-phenylindole; blue). Arrows indicate BGN in the glycocalyx and in the subendothelial space in close proximity to the endothelial cell layer. Data represent mean±SD. Scale bar, 10 µm. L indicates vessel lumen. *P<0.05 vs w/o CHD/stable CHD.

microscopy and apotome technology. To further validate the presence of biglycan in the glycocalyx of capillaries, confocal microscopy was performed. Figure III in the online-only Data Supplement clearly demonstrates luminal biglycan deposition in the glycocalyx of cardiac capillaries of *ApoE*-deficient mice. Larger vessels such as arterioles and venules were defined by isolectin- or CD31-positive cells forming lumina ≥25 µm. In contrast to capillaries, biglycan was absent from the endothelial glycocalyx of arterioles (Figure 1F). However, arterioles were characterized by pronounced deposition of biglycan in the subendothelial matrix (Figure 1F). In arterioles of *ApoE*$^{-/-}$/*Bgn*$^{-/0}$ mice, biglycan was not detected (Figure 1G). Thus, a large biglycan-rich vascular compartment exists in *ApoE*$^{-/-}$ mice that may mediate luminal and subendothelial activation of HCII in addition to possible activation of HCII by soluble circulating biglycan. Therefore, the vascular biglycan-rich extracellular matrix of small vessels may counteract thrombin activation and may function as an endogenous mechanism to protect from exaggerated thrombin activation.

Activation of Thrombin and Platelets in *ApoE*$^{-/-}$/*Bgn*$^{-/0}$ Mice

Next it was tested, whether deletion of biglycan affected thrombin generation in *ApoE*$^{-/-}$ mice. Thrombin generation in plasma was determined with automated thrombography. As shown in Figure 2, the endogenous thrombin potential (ETP) was increased in *ApoE*$^{-/-}$/*Bgn*$^{-/0}$ mice, a finding indicating increased thrombin activation in the absence of biglycan (Figure 2A–2C). The kinetics of thrombin formation was not changed (Figure 2D and 2E). The direct causality was shown by spiking the plasma of *ApoE*$^{-/-}$/*Bgn*$^{-/0}$ mice with DS causing reduced ETP. In contrast, spiking the plasma with biglycan core protein without DS side chains did not lead to reduction of increased ETP in *ApoE*$^{-/-}$/*Bgn*$^{-/0}$ mice. Furthermore, DS-induced ETP-reduction was blunted after digestion of DS with chondroitinase ABC, thereby underlining the importance of DS side chains for the biglycan-mediated activation of HCII (Figure 2F). Potential contamination of DS with heparins was excluded by digestion of DS with heparinase I/III showing no effect on DS-induced decrease in the ETP (Figure 2G and 2H).

Because the interaction between HCII and DS leads to thrombin inhibition, the level of HCII/thrombin complexes in plasma of *ApoE*- and *ApoE/Bgn* double-deficient mice was determined. Figure 2I shows that HCII/thrombin was indeed significantly decreased in *ApoE/Bgn* double-deficient mice.

Thrombin is an important activator of platelets. Therefore, intravital microscopy of platelet adhesion was performed in the uninjured *A. carotis communis* of either *ApoE*$^{-/-}$ or *ApoE*$^{-/-}$/*Bgn*$^{-/0}$ mice. Indeed, *ApoE*$^{-/-}$ platelets showed increased rolling on the endothelium of *ApoE/Bgn* double-deficient mice (Figure 2J). This effect was paralleled by increased surface expression of CD62P in thrombocytes, as determined by flow cytometric analysis, indicating increased platelet activation (Figure 2K).

To identify a possible prothrombotic phenotype in *ApoE*$^{-/-}$/*Bgn*$^{-/0}$ mice, occlusive thrombus formation in a photochemical model of arterial thrombosis with the photosensitizing dye Rose Bengal and tail bleeding time were analyzed. However, in both models, no hemostatic differences between *ApoE*$^{-/-}$ or

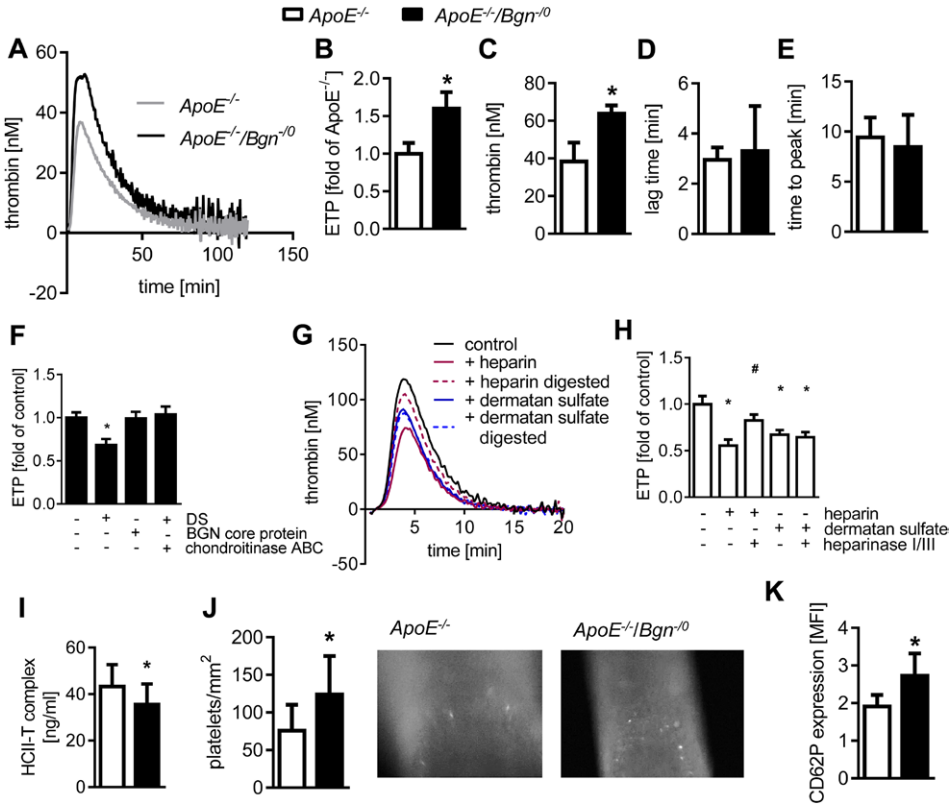

Figure 2. Increased thrombin generation and platelet activation in mice double-deficient in *ApoE* and *Bgn*. Thrombin generation was measured in plasma from 15-wk-old *ApoE*$^{-/-}$ and *ApoE*$^{-/-}$/*Bgn*$^{-/0}$ mice by determining the endogenous thrombin potential (ETP). **A** and **B**, Representative measurement of thrombin generation and respective endogenous thrombin potential (ETP). **C**–**E**, Peak height, lag time, and time to peak are shown; n=4. **F**, Analysis of the ETP in *ApoE*$^{-/-}$/*Bgn*$^{-/0}$ plasma after incubation with dermatan sulfate (DS; 10 μg/mL), biglycan (BGN) core protein (10 μg/mL) or chondroitinase ABC (0.02 U)–digested DS; n=3 to 4. **G**, Thrombin generation in *ApoE*-deficient mice after treatment with heparin and dermatan sulfate and with heparinase I/III–digested heparin and dermatan sulfate and (**H**) endogenous thrombin potential calculated as area under the curve; n=5. **I**, Heparin cofactor II–thrombin (HCII–T) complex in plasma of *ApoE*$^{-/-}$ and *ApoE*$^{-/-}$/*Bgn*$^{-/0}$ mice, n=11, 15. **J**, Intravital microscopy of platelet adhesion on the endothelium of *ApoE*$^{-/-}$ and *ApoE*$^{-/-}$/*Bgn*$^{-/0}$ mice. Quantification of rolling platelets and representative images of the common carotid artery are shown. n=10, 14. **K**, Basal activation of resting platelets was determined by flow cytometric analysis of CD62P expression; n=7, 8. Data represent mean±SD, **P*<0.05 vs *ApoE*$^{-/-}$ control mice or unstimulated *ApoE*$^{-/-}$/*Bgn*$^{-/0}$ control, #*P*<0.05 vs + heparin.

ApoE$^{-/-}$/*Bgn*$^{-/0}$ mice were detectable (Figure IV in the online-only Data Supplement).

Increased Macrophage-Mediated Plaque Inflammation in *ApoE*$^{-/-}$/*Bgn*$^{-/0}$ Mice

To determine possible consequences of increased thrombin and platelet activation for atherosclerosis, flow cytometry was used to analyze the immune cell populations in the aortas of 15-week-old *ApoE*$^{-/-}$/*Bgn*$^{-/0}$ double-deficient mice and littermate controls. This analysis revealed no differences in aortic weight and yield of living cells (Figure VA and VB in the online-only Data Supplement). Importantly, a higher macrophage content, as evidenced by the number of CD11b^{+}/F4/80^{+} cells (Figure 3A and 3B), was detected in *ApoE*$^{-/-}$/*Bgn*$^{-/0}$ mice. A representative gating scheme is depicted in Figure VI in the online-only Data Supplement. The numbers of total leukocytes, lymphocytes, B cells, T cells, and neutrophils did not differ between the genotypes (Figure VC–VG in the online-only Data Supplement).

To further corroborate the finding of increased macrophage presence in vascular lesions, the macrophage content of atherosclerotic lesions at the aortic root was determined by immunohistochemistry. During early atherosclerosis (in mice aged 15 weeks), macrophage content, as indicated by immunostaining of Mac-2 and F4/80, was strongly increased in *ApoE*$^{-/-}$/*Bgn*$^{-/0}$ mice (Figure 3C–3F). In line with a proinflammatory macrophage-driven phenotype, the concentrations of circulating monocyte chemotactic protein-1, monocyte inflammatory protein-1α, interleukin (IL)-2, and IL-3 were higher in *ApoE*$^{-/-}$/*Bgn*$^{-/0}$ mice than in *ApoE*$^{-/-}$ mice. The concentrations of other cytokines, such as IL-4 and IL-6, showed strong trends toward downregulation. The concentration of tumor necrosis factor-α was unaffected. In addition, anti-inflammatory IL-10 was upregulated possibly as a part of a counter regulatory adaptation (Figure 3G).

Increased Atherosclerosis in *ApoE*$^{-/-}$/*Bgn*$^{-/0}$ Mice

The extent of atherosclerosis was determined in mice aged 15 and 30 weeks. In line with enhanced thrombin generation and macrophage-driven inflammation, both the plaque burden in the aorta and the plaque size at the aortic root were significantly higher in 30-week-old *ApoE*$^{-/-}$/*Bgn*$^{-/0}$ mice (Figure 4A–4D). To corroborate the conclusion of a proatherosclerotic effect of biglycan deficiency, mice double-deficient in *Ldl receptor* and *Bgn* (*Ldlr*$^{-/-}$/*Bgn*$^{-/0}$) were fed a Western-type diet

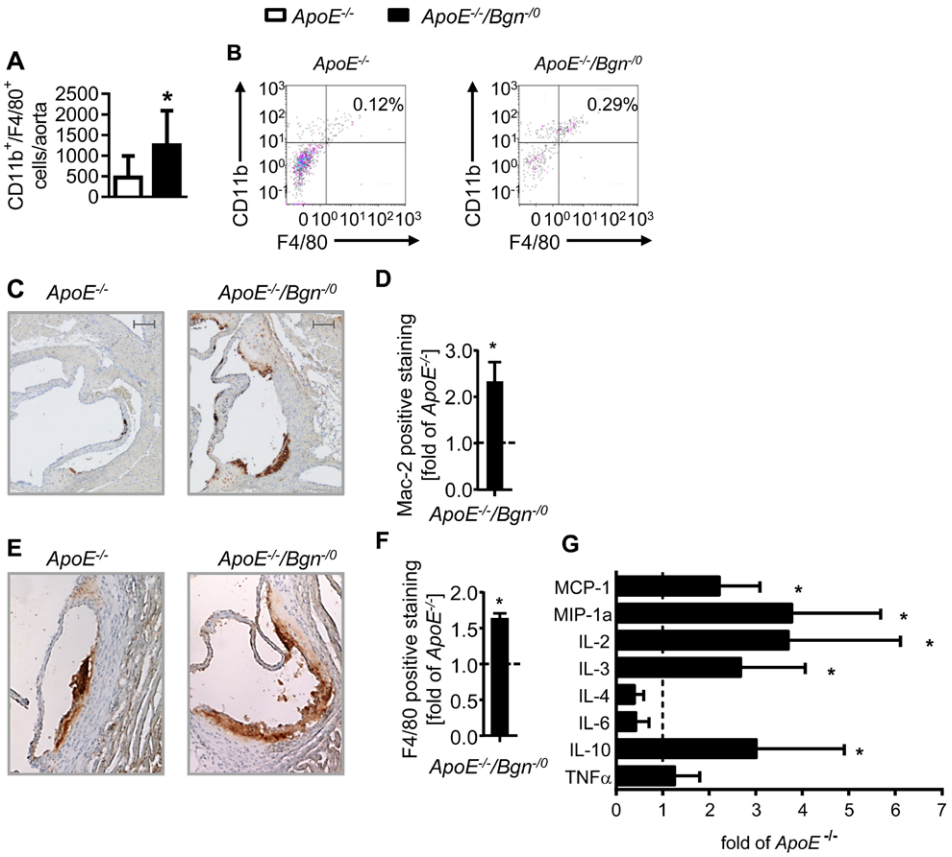

Figure 3. Increased macrophage content in aortas and aortic root plaques and elevation in circulating cytokines of *ApoE*/*Bgn* double-deficient mice. **A**, Flow cytometric analysis of aortic CD11b$^+$/F4/80$^+$ macrophages of *ApoE*$^{-/-}$ and *ApoE*$^{-/-}$/*Bgn*$^{-/0}$ mice at 15 wk of age; n=6, 4. **B**, Representative flow cytometric plots of CD11b$^+$/F4/80$^+$ macrophages gated on living CD45$^+$ cells with percentages of CD11b$^{+/}$F4/80$^+$ macrophages of living cells are shown. A representative gating scheme is provided in Figure VI in the online-only Data Supplement. **C** and **D**, Immunohistochemical analysis detected Mac-2–positive cells in cross sections of the aortic roots of 15-wk-old *ApoE*$^{-/-}$ and *ApoE*$^{-/-}$/*Bgn*$^{-/0}$ mice; n=7, 8. **E** and **F**, Immunohistochemical analysis of F4/80 as a marker of mature macrophages in 15-wk-old *ApoE*$^{-/-}$ and *ApoE*$^{-/-}$/*Bgn*$^{-/0}$ mice; n=4, 5. **G**, Circulating plasma concentrations of chemokines and cytokines were measured by Q-Plex Mouse Cytokine–Screen IR; n=5, 3. Data represent mean±SD, **P*<0.05 as compared with *ApoE*$^{-/-}$ control mice. Scale bar, 100 μm. IL indicates interleukin; MCP, monocyte chemotactic protein; MIP, monocyte inflammatory protein; and TNF, tumor necrosis factor.

and analyzed. These mice develop severe aortic aneurysms as previously shown by Tang et al.[19] Indeed, increased plaques at the aortic root (Figure 4E) and increased macrophage-driven inflammation were detected in these mice (Figure 4F). Thus, the key finding of increased atherosclerosis and increased macrophage-mediated inflammation in the absence of biglycan was confirmed in a second model of murine atherosclerosis.

Remodeling of Atherosclerotic Plaques in *ApoE*$^{-/-}$/*Bgn*$^{-/0}$ Mice

Alterations in the proteoglycan composition of the plaque matrix were sought in an unbiased approach through mass spectrometry in mice aged 15 weeks. As expected, biglycan was not detectable in aortas from *ApoE*$^{-/-}$/*Bgn*$^{-/0}$ mice. In addition, the expression of decorin, perlecan, and versican was unchanged (Figure 5; complete proteomic data sets in Tables II and III in the online-only Data Supplement). Unexpectedly, the signal for the chondroitin sulfate proteoglycan aggrecan, which is typical of cartilage matrix, was increased. Furthermore, the expression of the proteoglycan prolargin was decreased. Immunostaining confirmed unaltered expression of decorin and versican and a trend toward increased expression of perlecan. In line with mass spectrometry, IHC staining of aggrecan detected an increase in aggrecan expression. The expression of prolargin was only slightly decreased in plaques at the aortic root (Figure 5A–5C).

Interestingly, increased numbers of α-smooth muscle actin–positive cells were detected in aortic root plaques from *ApoE*$^{-/-}$/*Bgn*$^{-/0}$ mice (Figure 5D). Whether these cells originate from vascular SMC, macrophages, or pericytes cannot be concluded from the present data.[20] There were no differences between the genotypes in 5-bromo-2′-deoxyuridine incorporation (Figure 5E).

Lipid retention as evidenced by ApoB-48/100 retention and Oil-Red-O staining in aortic root plaques was not changed in atherosclerotic plaques of *ApoE*$^{-/-}$/*Bgn*$^{-/0}$ mice (Figure VII in the online-only Data Supplement).

Pharmacological Thrombin Inhibition Alleviates Platelet Activation and Inflammation in *ApoE*$^{-/-}$/*Bgn*$^{-/0}$ Mice

The findings presented to date suggest that biglycan plays a role in balancing thrombin activity in *ApoE*-deficient mice and thereby moderates the progression of atherosclerosis in this model. This hypothesis was tested by treating *ApoE*$^{-/-}$ and

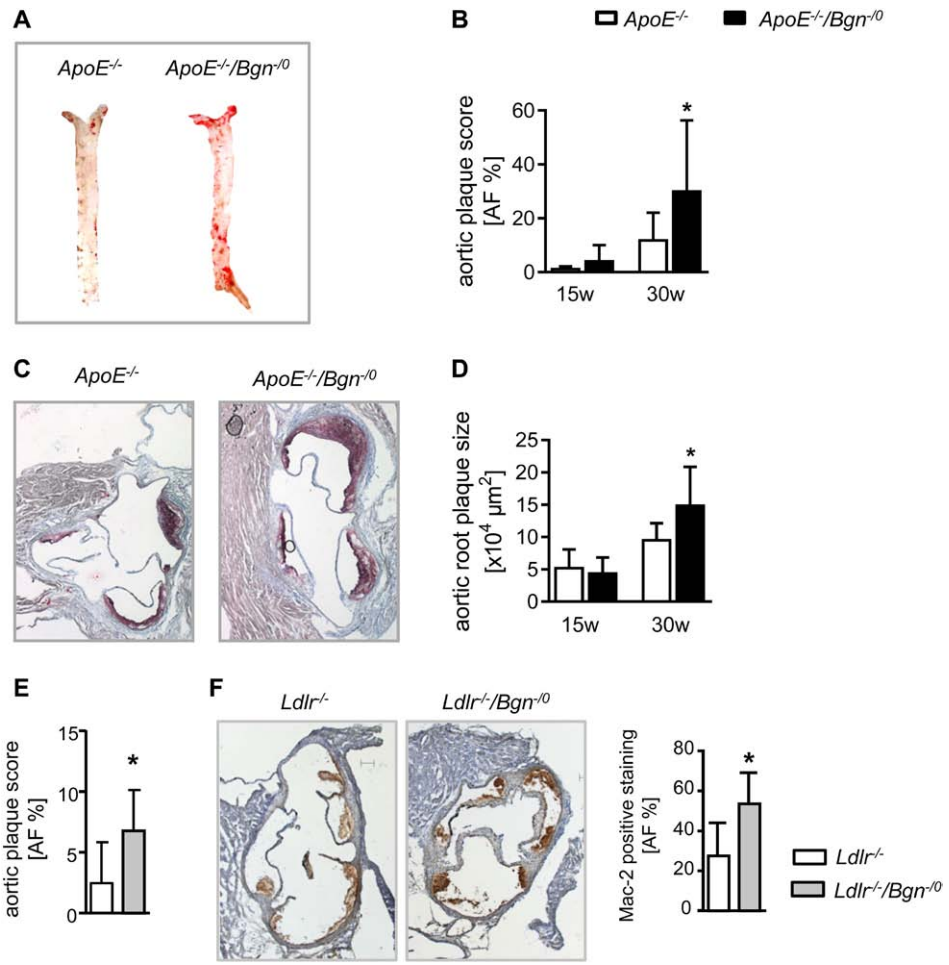

Figure 4. Increased atherosclerosis in *ApoE /Bgn- and Ldlr/Bgn* double-deficient mice. The aortas of 15- and 30-wk-old old *ApoE*$^{-/-}$ and *ApoE*$^{-/-}$/*Bgn*$^{-/0}$ mice were stained with Oil Red O, and the plaque burden was quantified with ImageJ software. **A**, Representative pictures of Oil-Red-O–stained en face preparations of the aorta of 30-wk-old *ApoE*$^{-/-}$ and *ApoE*$^{-/-}$/*Bgn*$^{-/0}$ mice. **B**, A strong increase in the atherosclerotic plaque score was detected in the 30-wk-old *ApoE*$^{-/-}$/*Bgn*$^{-/0}$ mice; 15-wk-old mice, n=12, 11; 30-wk-old mice, n=15, 16. **C** and **D**, Plaque size at the aortic root was determined in 10 cross sections per animal from 15- and 30-wk-old mice; 15-wk-old mice, n=6, 8; 30-wk-old mice, n=8, 13. **E** and **F**, As a proof of concept, atherosclerotic plaque burden was also determined in male *Ldlr/Bgn* double-deficient mice after 6 wk on a Western diet. **E**, Plaque score by aortic en face staining with Oil Red O. **F**, Increased Mac-2 staining in the aortic root lesions. n=6, 7. Data represent mean±SD, **P*<0.05 vs respective control mice. Scale bar, 100 µm. AF indicates area fraction.

ApoE$^{-/-}$/*Bgn*$^{-/0}$ mice with the thrombin inhibitor argatroban (0.6 mg/kg per day) or respective vehicle for 7 weeks. No argatroban-mediated effect on circulating biglycan was detectable in plasma of *ApoE*-deficient mice (Figure VIII in the online-only Data Supplement). However, platelet activation, as evidenced by CD62P expression, was reduced in *ApoE*$^{-/-}$/*Bgn*$^{-/0}$ mice receiving argatroban (Figure 6A). Plaque size at the aortic root was significantly decreased in *ApoE*$^{-/-}$/*Bgn*$^{-/0}$ mice treated with argatroban when compared with the vehicle control group (Figure 6B). In addition, flow cytometric analysis of the aorta (Figure 6C and 6D) revealed a significant decrease in the numbers of aortic macrophages in response to argatroban. These results strongly suggest that increased thrombin activity was indeed the underlying cause of increased plaque inflammation and subsequent atherosclerosis in *ApoE*$^{-/-}$/*Bgn*$^{-/0}$ mice.

Discussion

This study found that genetic deletion of *Bgn* aggravates the development of atherosclerosis. The increase in plaque burden was seen in 2 models of atherosclerosis, *ApoE*$^{-/-}$/*Bgn*$^{-/0}$ mice and *Ldlr*$^{-/-}$/*Bgn*$^{-/0}$ double-deficient mice. Therefore, the current findings add important new information about the role of biglycan in atherosclerosis. To date, biglycan has been suspected of contributing to atheroprogression. The results of our studies showed that biglycan functions in atherosclerosis as a matrix-derived inhibitor of thrombin, thereby decreasing total thrombin activity and subsequent downstream events such as platelet activation and inflammation. This is based on the activation of HCII by the DS chains of biglycan[21,22] and, in turn, inactivation of active thrombin. Importantly, biglycan-mediated thrombin inhibition does not mediate hemostatic effects because no effects on bleeding time and arterial thrombus formation were observed. From a translational perspective, biglycan may thereby affect cardiovascular risk and change the response to pharmacological interventions and may itself be a (pleiotropic) target of cardiovascular drugs. Specifically, it may be considered that patients with low biglycan—as reported for patients with low

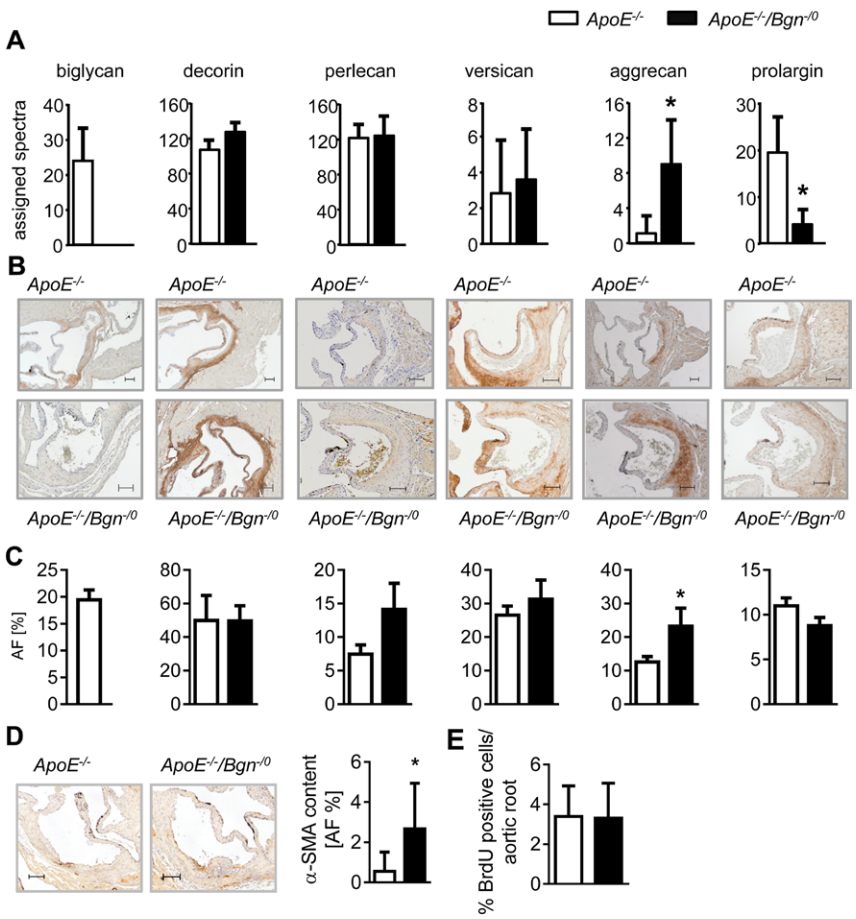

Figure 5. Mass spectrometric analysis of aortic extracellular matrix (ECM) and alterations in plaque composition at the aortic root of *ApoE*$^{-/-}$/*ApoE*$^{-/-}$/*Bgn*$^{-/0}$ mice. **A**, Aortas of 15-wk-old *ApoE*$^{-/-}$ and *ApoE*$^{-/-}$/*Bgn*$^{-/0}$ mice were harvested and subjected to mass spectrometric analysis of ECM proteins. Depicted are proteoglycans selected on the basis of the assignment of spectra after mass spectrometry. n=5, 4. **B**, Immunohistochemical analysis of biglycan, decorin, perlecan, versican, aggrecan, and prolargin at the aortic root of *ApoE*$^{-/-}$ and *ApoE*$^{-/-}$/*Bgn*$^{-/0}$ mice and, **C**, respective quantification using ImageJ software; n=3 to 5. **D**, The amount of α-smooth muscle actin (α-SMA) was quantified by ImageJ analysis; n=11, 7. **E**, Positive 5-bromo-2′-deoxyuridine (BrdU) immunostaining at the aortic root was used to determine proliferative activity; n=9, 7. Data represent mean±SD, **P*<0.05 vs *ApoE*$^{-/-}$ mice. Scale bar, 100 μm. AF indicates area fraction.

HCII expression—and therefore higher thrombin activity may be at a higher cardiovascular risk and that the response to non–vitamin K-dependent oral anticoagulants might be modulated by the level of endogenous thrombin inhibition. Currently, the use of non–vitamin K-dependent oral anticoagulants to treat acute coronary syndrome is being considered as an addition to single- or dual-antiplatelet therapy.[23,24] Furthermore, biglycan content is regulated by statins, angiotensin type 1 receptor antagonists, and likely other drugs that are regularly used to treat patients at high risk of cardiovascular events.[18,25,26]

No previous studies have addressed the question whether biglycan circulates in patients with coronary heart disease or in *ApoE*$^{-/-}$ mice. Interestingly, the current study found that circulating concentrations of biglycan are increased in *ApoE*$^{-/-}$ mice and in patients with acute coronary syndrome. Because biglycan content is also regulated by different external factors as described above, possible confounding influences in the analysis of human plasma samples by, eg, comorbidities and medication, cannot be completely ruled out. However, no obvious differences between the 3 patient groups were observed. The biological function of circulating biglycan in atherosclerosis has not yet been clarified, but in light of the current results, it may be interpreted as an antithrombotic counterregulation in the proatherosclerotic state. In addition, activated endothelial cells strongly express biglycan,[27] and it is shown here that biglycan-rich extracellular matrix is present as a part of the luminal glycocalyx of capillaries. This may be of particular interest because it creates an enormous surface for 2-dimensional interactions of circulating HCII and DS-GAG chains of biglycan. This would be analogous to the interaction of antithrombin III and the heparan sulfate that also takes place in the endothelial glycocalyx[28] and adds a new mechanism for balancing hemostasis. In addition, it is shown here that biglycan is present in large amounts in the subendothelial space in arterioles. Therefore, endothelial cell–derived biglycan may provide a large compartment that facilitates biglycan/HCII interactions and could thereby inhibit thrombin activity and platelet function systemically. Circumstantial evidence from published studies points toward a local antithrombotic effect of vascular biglycan because the fibrous cap of thrombosed human eroded plaques is devoid of biglycan.[12]

In human atherosclerosis, DS chains of biglycan are thought to be altered in a way that HCII activation is reduced.[8] Importantly, reduced HCII expression has been associated with aggravated atherosclerosis in humans.[29,30] Mechanistically, this reduced expression of HCII may lead to increased thrombin-mediated activation of platelets, which in turn stimulate macrophage-mediated inflammation.[31,32] As shown here, the absence of biglycan in *ApoE*$^{-/-}$/*Bgn*$^{-/0}$ mice causes increased thrombin activity and subsequently increased plaque inflammation. The extent of thrombin activation in *ApoE*$^{-/-}$/*Bgn*$^{-/0}$ mice did, however, not lead to changes in hemostasis or an overt thrombotic phenotype. However, because thrombosis models involve endothelial injury and denudation, this leads

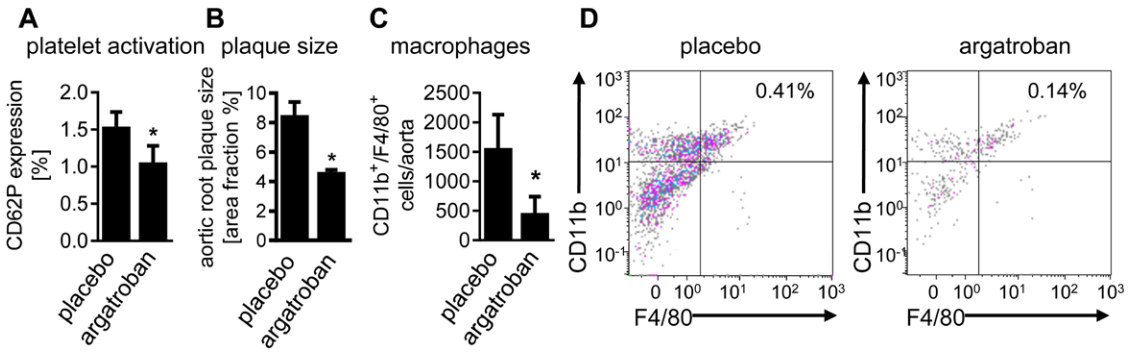

Figure 6. Argatroban reverses platelet activation and macrophage accumulation in *ApoE*$^{-/-}$/*Bgn*$^{-/0}$ mice. Mice were treated for 7 wk with argatroban (0.6 mg/kg per day) and evaluated at 15 wk of age. **A**, Activation of platelets was determined by flow cytometric analysis of CD62P expression; n=4, 3. **B**, The plaque size in the aortic root was calculated from 3 different sections in 15-wk-old mice; n=6, 3. **C**, Flow cytometric analysis of macrophages in the aortas of 15-wk-old *ApoE*$^{-/-}$/*Bgn*$^{-/0}$ mice and (**D**) representative plots of CD11b^{+}/F4/80^{+} macrophages gated on living CD45^{+} cells. Shown are CD11b^{+}/F4/80^{+} macrophages as % of living cells; n=5, 3. Data represent mean±SD, **P*<0.05 vs placebo-treated mice.

to collagen exposure and therefore strongly activates both platelets and the coagulation cascade. It is likely that such a strong activation of the hemostatic cascade will overwrite the lack of biglycan/HCII-mediated thrombin inhibition.

In line with a causal role of enhanced thrombin activity, it was demonstrated here that argatroban treatment reduced platelet activation and plaque inflammation in *ApoE*$^{-/-}$/*Bgn*$^{-/0}$ mice. In support of this hypothesis are findings indicating that activated platelets and increased platelet adhesion contribute to atheroprogression in *the ApoE*$^{-/-}$ model[33] and that *HCII/ApoE* double-deficient mice develop increased atherosclerosis.[34] From a translational viewpoint, *ApoE*$^{-/-}$/*Bgn*$^{-/0}$ mice are a new model of systemic thrombin and platelet activation.

The current findings strongly suggest that increased thrombin activity and plaque inflammation caused by the absence of biglycan in the *ApoE*$^{-/-}$ knockout background account for the proatherosclerotic phenotype. A proinflammatory macrophage phenotype was evidenced by increased concentrations of circulating cytokines and increased numbers of macrophages in atherosclerotic lesions. In addition, it may be of importance that biglycan itself is an agonist of toll-like receptor-2 and toll-like receptor-4.[15] Therefore, the absence of this abundant toll-like receptor ligand may render macrophages hypersensitive to stimulation with other toll-like receptor ligands, such as hyaluronan.[35] Hyaluronan and the hyaluronan-binding proteoglycan versican are also abundant in atherosclerotic plaque[36] and were detected in atherosclerotic lesions in the present study.

Previous studies have shown that *Bgn* knockout mice exhibit a defect in bone formation and mineralization that is accompanied by inflammation and that cumulates in an osteoarthritic/osteoporotic phenotype.[37,38] In our recent study, we found that the infusion of angiotensin-II into *Ldlr/Bgn* double-deficient mice causes severe abdominal aneurysms, a finding that again suggests that biglycan plays a protective role against maladaptive vessel remodelling.[19]

Of note, the amount of lipid retention was unaffected although biglycan has been considered to be a lipoprotein-binding proteoglycan and to contribute thereby to the retention of lipoproteins.[39] Specifically, in vitro, in SMCs, it was shown that overexpression of biglycan increases low-density lipoprotein-binding.[40] This was confirmed by increased lipid retention in *Ldlr*$^{-/-}$ mice after overexpression of biglycan in SMCs.[41] Furthermore, it has been shown that biglycan contributes to the subendothelial accumulation of lipoprotein during early intimal thickening in humans because biglycan is expressed at sites of subsequent lipid deposition and macrophage accumulation.[16] These findings clearly indicated that biglycan can mediate low-density lipoprotein retention. However, the present study shows that genetic deletion of *Bgn* does not lead to reduced low-density lipoprotein-retention and atherosclerosis, likely because of the availability of sufficient negatively charged glycosaminoglycan chains from other proteoglycans. This conclusion was based on the present mass spectrometric and immunohistochemical analysis of vascular proteoglycans showing that the amounts of versican, perlecan, and decorin did not differ in *ApoE*$^{-/-}$/*Bgn*$^{-/0}$ mice.[16] Furthermore, upregulation of aggrecan was detected, which may contribute additional negatively charged glycosaminoglycan chains to compensate for the deletion of biglycan. Therefore, it is concluded that biglycan is not the limiting factor in intimal lipoprotein binding and that the other proteoglycans substitute for biglycan by offering sufficient binding sides for lipoproteins at least in advanced atherosclerosis. The conclusion that the absence of biglycan does not crucially affect lipoprotein retention in atherosclerotic plaques is also supported by the observation that chronic treatment with statins dramatically increases the concentrations of biglycan in atherosclerotic plaques without affecting the retention of lipoproteins in late atherosclerosis.[18] Comparing human atherosclerosis-prone internal carotid arteries with atherosclerosis-resistant internal thoracic arteries found no difference in biglycan content.[42] However, the current findings do not rule out the possibility that biglycan contributes to the subendothelial accumulation of lipoprotein during early intimal thickening in humans because biglycan is expressed at sites of subsequent lipid deposition and macrophage accumulation.[16]

In conclusion, this study provides clear evidence that genetic deletion of *Bgn* is detrimental with respect to atherosclerosis in mice. Biglycan circulates and is present in the endothelial glycocalyx and subendothelial matrix and is identified as a relevant endogenous inhibitor of thrombin

generation in murine atherosclerosis. Specifically, the deletion of *Bgn* increases thrombin activity and platelet activation without influencing hemostasis, but in turn contributes to increased inflammation of plaques and more rapid progression of atherosclerosis.

Acknowledgments

We thank Annika Zimmermann, Kerstin Freidel, and Petra Rompel for excellent technical assistance. We also thank Stephanie Weidtkamp-Peters, Center for advanced imaging (CAi) Düsseldorf, for technical assistance with the confocal laser scanning system.

Sources of Funding

This work was supported by the Deutsche Forschungsgemeinschaft (IRTG 1902, SFB1116, SFB815, SFB 1039, and SCHA 1082/6-1).

Disclosures

None.

References

1. Zheng L, Martins-Green M. Molecular mechanisms of thrombin-induced interleukin-8 (IL-8/CXCL8) expression in THP-1-derived and primary human macrophages. *J Leukoc Biol*. 2007;82:619–629. doi: 10.1189/jlb.0107009.
2. Huo Y, Schober A, Forlow SB, Smith DF, Hyman MC, Jung S, Littman DR, Weber C, Ley K. Circulating activated platelets exacerbate atherosclerosis in mice deficient in apolipoprotein E. *Nat Med*. 2003;9:61–67. doi: 10.1038/nm810.
3. Oldgren J, Wallentin L, Alexander JH, James S, Jönelid B, Steg G, Sundström J. New oral anticoagulants in addition to single or dual antiplatelet therapy after an acute coronary syndrome: a systematic review and meta-analysis. *Eur Heart J*. 2013;34:1670–1680. doi: 10.1093/eurheartj/eht049.
4. Kornerup KN, Salmon GP, Pitchford SC, Liu WL, Page CP. Circulating platelet-neutrophil complexes are important for subsequent neutrophil activation and migration. *J Appl Physiol (1985)*. 2010;109:758–767. doi: 10.1152/japplphysiol.01086.2009.
5. Colotta F, Sciacca FL, Sironi M, Luini W, Rabiet MJ, Mantovani A. Expression of monocyte chemotactic protein-1 by monocytes and endothelial cells exposed to thrombin. *Am J Pathol*. 1994;144:975–985.
6. Aihara K, Azuma H, Takamori N, Kanagawa Y, Akaike M, Fujimura M, Yoshida T, Hashizume S, Kato M, Yamaguchi H, Kato S, Ikeda Y, Arase T, Kondo A, Matsumoto T. Heparin cofactor II is a novel protective factor against carotid atherosclerosis in elderly individuals. *Circulation*. 2004;109:2761–2765. doi: 10.1161/01.CIR.0000129968.46095.F3.
7. Ise T, Aihara K, Sumitomo-Ueda Y, Yoshida S, Ikeda Y, Yagi S, Iwase T, Yamada H, Akaike M, Sata M, Matsumoto T. Plasma heparin cofactor II activity is inversely associated with left atrial volume and diastolic dysfunction in humans with cardiovascular risk factors. *Hypertens Res*. 2011;34:225–231. doi: 10.1038/hr.2010.211.
8. Shirk RA, Parthasarathy N, San Antonio JD, Church FC, Wagner WD. Altered dermatan sulfate structure and reduced heparin cofactor II-stimulating activity of biglycan and decorin from human atherosclerotic plaque. *J Biol Chem*. 2000;275:18085–18092. doi: 10.1074/jbc.M001659200.
9. Chang MY, Potter-Perigo S, Tsoi C, Chait A, Wight TN. Oxidized low density lipoproteins regulate synthesis of monkey aortic smooth muscle cell proteoglycans that have enhanced native low density lipoprotein binding properties. *J Biol Chem*. 2000;275:4766–4773.
10. Tiede K, Melchior-Becker A, Fischer JW. Transcriptional and posttranscriptional regulators of biglycan in cardiac fibroblasts. *Basic Res Cardiol*. 2010;105:99–108. doi: 10.1007/s00395-009-0049-8.
11. Schaefer L, Macakova K, Raslik I, Micegova M, Gröne HJ, Schönherr E, Robenek H, Echtermeyer FG, Grässel S, Bruckner P, Schaefer RM, Iozzo RV, Kresse H. Absence of decorin adversely influences tubulointerstitial fibrosis of the obstructed kidney by enhanced apoptosis and increased inflammatory reaction. *Am J Pathol*. 2002;160:1181–1191. doi: 10.1016/S0002-9440(10)64937-1.
12. Kolodgie FD, Burke AP, Farb A, Weber DK, Kutys R, Wight TN, Virmani R. Differential accumulation of proteoglycans and hyaluronan in culprit lesions: insights into plaque erosion. *Arterioscler Thromb Vasc Biol*. 2002;22:1642–1648.
13. Corsi A, Xu T, Chen XD, Boyde A, Liang J, Mankani M, Sommer B, Iozzo RV, Eichstetter I, Robey PG, Bianco P, Young MF. Phenotypic effects of biglycan deficiency are linked to collagen fibril abnormalities, are synergized by decorin deficiency, and mimic Ehlers-Danlos-like changes in bone and other connective tissues. *J Bone Miner Res*. 2002;17:1180–1189. doi: 10.1359/jbmr.2002.17.7.1180.
14. Babelova A, Moreth K, Tsalastra-Greul W, Zeng-Brouwers J, Eickelberg O, Young MF, Bruckner P, Pfeilschifter J, Schaefer RM, Gröne HJ, Schaefer L. Biglycan, a danger signal that activates the NLRP3 inflammasome via toll-like and P2X receptors. *J Biol Chem*. 2009;284:24035–24048. doi: 10.1074/jbc.M109.014266.
15. Schaefer L, Babelova A, Kiss E, Hausser HJ, Baliova M, Krzyzankova M, Marsche G, Young MF, Mihalik D, Götte M, Malle E, Schaefer RM, Gröne HJ. The matrix component biglycan is proinflammatory and signals through Toll-like receptors 4 and 2 in macrophages. *J Clin Invest*. 2005;115:2223–2233. doi: 10.1172/JCI23755.
16. Nakashima Y, Fujii H, Sumiyoshi S, Wight TN, Sueishi K. Early human atherosclerosis: accumulation of lipid and proteoglycans in intimal thickenings followed by macrophage infiltration. *Arterioscler Thromb Vasc Biol*. 2007;27:1159–1165. doi: 10.1161/ATVBAHA.106.134080.
17. O'Brien KD, Olin KL, Alpers CE, Chiu W, Ferguson M, Hudkins K, Wight TN, Chait A. Comparison of apolipoprotein and proteoglycan deposits in human coronary atherosclerotic plaques: colocalization of biglycan with apolipoproteins. *Circulation*. 1998;98:519–527.
18. Marzoll A, Melchior-Becker A, Cipollone F, Fischer JW. Small leucine-rich proteoglycans in atherosclerotic lesions: novel targets of chronic statin treatment? *J Cell Mol Med*. 2011;15:232–243. doi: 10.1111/j.1582-4934.2009.00986.x.
19. Tang T, Thompson JC, Wilson PG, Yoder MH, Müeller J, Fischer JW, Williams KJ, Tannock LR. Biglycan deficiency: increased aortic aneurysm formation and lack of atheroprotection. *J Mol Cell Cardiol*. 2014;75:174–180. doi: 10.1016/j.yjmcc.2014.07.014.
20. Shankman LS, Gomez D, Cherepanova OA, Salmon M, Alencar GF, Haskins RM, Swiatlowska P, Newman AA, Greene ES, Straub AC, Isakson B, Randolph GJ, Owens GK. KLF4-dependent phenotypic modulation of smooth muscle cells has a key role in atherosclerotic plaque pathogenesis. *Nat Med*. 2015;21:628–637. doi: 10.1038/nm.3866.
21. Whinna HC, Choi HU, Rosenberg LC, Church FC. Interaction of heparin cofactor II with biglycan and decorin. *J Biol Chem*. 1993;268:3920–3924.
22. Tollefsen DM, Pestka CA, Monafo WJ. Activation of heparin cofactor II by dermatan sulfate. *J Biol Chem*. 1983;258:6713–6716.
23. Mega JL, Braunwald E, Wiviott SD, et al.; ATLAS ACS 2–TIMI 51 Investigators. Rivaroxaban in patients with a recent acute coronary syndrome. *N Engl J Med*. 2012;366:9–19. doi: 10.1056/NEJMoa1112277.
24. Alexander JH, Lopes RD, James S, et al.; APPRAISE-2 Investigators. Apixaban with antiplatelet therapy after acute coronary syndrome. *N Engl J Med*. 2011;365:699–708. doi: 10.1056/NEJMoa1105819.
25. Nagy N, Melchior-Becker A, Fischer JW. Long-term treatment with the AT1-receptor antagonist telmisartan inhibits biglycan accumulation in murine atherosclerosis. *Basic Res Cardiol*. 2010;105:29–38. doi: 10.1007/s00395-009-0051-1.
26. Nigro J, Potter-Perigo S, Ivey ME, de Dios ST, Evanko SP, Wight TN, Little PJ. The effect of PPAR ligands to modulate glucose metabolism alters the incorporation of metabolic precursors into proteoglycans synthesized by human vascular smooth muscle cells. *Arch Physiol Biochem*. 2008;114:171–177. doi: 10.1080/13813450802181013.
27. Kinsella MG, Tsoi CK, Järveläinen HT, Wight TN. Selective expression and processing of biglycan during migration of bovine aortic endothelial cells. The role of endogenous basic fibroblast growth factor. *J Biol Chem*. 1997;272:318–325.
28. Okajima K. Antithrombin prevents endotoxin-induced pulmonary vascular injury by inhibiting leukocyte activation. *Blood Coagul Fibrinolysis*. 1998;9(suppl 2):S25–S37.
29. Kanagawa Y, Shigekiyo T, Aihara K, Akaike M, Azuma H, Matsumoto T. Molecular mechanism of type I congenital heparin cofactor (HC) II deficiency caused by a missense mutation at reactive P2 site: HC II Tokushima. *Thromb Haemost*. 2001;85:101–107.
30. Takamori N, Azuma H, Kato M, Hashizume S, Aihara K, Akaike M, Tamura K, Matsumoto T. High plasma heparin cofactor II activity is associated with reduced incidence of in-stent restenosis after percutaneous coronary intervention. *Circulation*. 2004;109:481–486. doi: 10.1161/01.CIR.0000109695.39671.37.

31. Borissoff JI, Otten JJ, Heeneman S, et al. Genetic and pharmacological modifications of thrombin formation in apolipoprotein e-deficient mice determine atherosclerosis severity and atherothrombosis onset in a neutrophil-dependent manner. *PLoS One*. 2013;8:e55784. doi: 10.1371/journal.pone.0055784.
32. Kastl SP, Speidl WS, Katsaros KM, Kaun C, Rega G, Assadian A, Hagmueller GW, Hoeth M, de Martin R, Ma Y, Maurer G, Huber K, Wojta J. Thrombin induces the expression of oncostatin M via AP-1 activation in human macrophages: a link between coagulation and inflammation. *Blood*. 2009;114:2812–2818. doi: 10.1182/blood-2009-01-200915.
33. Massberg S, Gawaz M, Grüner S, Schulte V, Konrad I, Zohlnhöfer D, Heinzmann U, Nieswandt B. A crucial role of glycoprotein VI for platelet recruitment to the injured arterial wall in vivo. *J Exp Med*. 2003;197:41–49.
34. Aihara K, Azuma H, Akaike M, et al. Strain-dependent embryonic lethality and exaggerated vascular remodeling in heparin cofactor II-deficient mice. *J Clin Invest*. 2007;117:1514–1526. doi: 10.1172/JCI27095.
35. Jiang D, Liang J, Fan J, et al. Regulation of lung injury and repair by Toll-like receptors and hyaluronan. *Nat Med*. 2005;11:1173–1179. doi: 10.1038/nm1315.
36. Wight TN, Merrilees MJ. Proteoglycans in atherosclerosis and restenosis: key roles for versican. *Circ Res*. 2004;94:1158–1167. doi: 10.1161/01.RES.0000126921.29919.51.
37. Ameye L, Young MF. Mice deficient in small leucine-rich proteoglycans: novel *in vivo* models for osteoporosis, osteoarthritis, Ehlers-Danlos syndrome, muscular dystrophy, and corneal diseases. *Glycobiology*. 2002;12:107R–116R.
38. Xu T, Bianco P, Fisher LW, et al. Targeted disruption of the biglycan gene leads to an osteoporosis-like phenotype in mice. *Nat Genet*. 1998;20:78–82. doi: 10.1038/1746.
39. Skålén K, Gustafsson M, Rydberg EK, Hultén LM, Wiklund O, Innerarity TL, Borén J. Subendothelial retention of atherogenic lipoproteins in early atherosclerosis. *Nature*. 2002;417:750–754. doi: 10.1038/nature00804.
40. O'Brien KD, Lewis K, Fischer JW, Johnson P, Hwang JY, Knopp EA, Kinsella MG, Barrett PH, Chait A, Wight TN. Smooth muscle cell biglycan overexpression results in increased lipoprotein retention on extracellular matrix: implications for the retention of lipoproteins in atherosclerosis. *Atherosclerosis*. 2004;177:29–35. doi: 10.1016/j.atherosclerosis.2004.07.007.
41. Thompson JC, Tang T, Wilson PG, Yoder MH, Tannock LR. Increased atherosclerosis in mice with increased vascular biglycan content. *Atherosclerosis*. 2014;235:71–75. doi: 10.1016/j.atherosclerosis.2014.03.037.
42. Talusan P, Bedri S, Yang S, Kattapuram T, Silva N, Roughley PJ, Stone JR. Analysis of intimal proteoglycans in atherosclerosis-prone and atherosclerosis-resistant human arteries by mass spectrometry. *Mol Cell Proteomics*. 2005;4:1350–1357. doi: 10.1074/mcp.M500088-MCP200.

Significance

Thrombin activates platelets and immune cells through protease-activated receptors and thereby stimulates vascular inflammation. States of enhanced thrombin activity, such as atherosclerosis and diabetes mellitus, are associated with chronic low-grade inflammation. Biglycan inhibits thrombin via its dermatan sulfate-rich side chains and activation of heparin cofactor II. Here, it is shown that biglycan localizes to the capillary glycocalyx and that plasma biglycan is elevated in *Apolipoprotein E*-deficient mice and in patients with acute coronary syndrome. Importantly, genetic deletion of *biglcyan* enhances thrombin activity, platelet activation, and macrophage-driven inflammation and thereby augments atherosclerosis in mice. Therefore, biglycan might counteract increased thrombin activation in atherosclerosis and thus mediates anti-inflammatory and atheroprotective effects.

Arteriosclerosis, Thrombosis, and Vascular Biology

JOURNAL OF THE AMERICAN HEART ASSOCIATION

Loss of *Biglycan* Enhances Thrombin Generation in *Apolipoprotein E*-Deficient Mice: Implications for Inflammation and Atherosclerosis

Maria Grandoch, Christina Kohlmorgen, Ariane Melchior-Becker, Kathrin Feldmann, Susanne Homann, Julia Müller, Lena-Sophia Kiene, Jinyang Zeng-Brouwers, Friederike Schmitz, Nadine Nagy, Amin Polzin, Nina S. Gowert, Margitta Elvers, Philipp Skroblin, Xiaoke Yin, Manuel Mayr, Liliana Schaefer, Lisa R. Tannock and Jens W. Fischer

Arterioscler Thromb Vasc Biol. 2016;36:e41-e50; originally published online March 31, 2016;
doi: 10.1161/ATVBAHA.115.306973
Arteriosclerosis, Thrombosis, and Vascular Biology is published by the American Heart Association, 7272 Greenville Avenue, Dallas, TX 75231

Print ISSN: 1079-5642. Online ISSN: 1524-4636

SUPPLEMENTAL MATERIAL

Material and Methods

Atherosclerosis model

Bgn knock-out mice (*Bgn*$^{-/0}$) on a C57BL/6J background were crossed into the *Apolipoprotein E*-deficient (*ApoE*$^{-/-}$) background. For the described experiments, a heterozygous breeding strategy was applied, and male *ApoE*$^{-/-}$/*Bgn*$^{-/0}$ mice and *ApoE*$^{-/-}$ littermates were used for the experiments. Both genotypes of mice were fed with normal chow and were examined at the age of 15 or 30 weeks. In addition, mice deficient in the low-density lipoprotein receptor (*Ldlr*$^{-/-}$) mice were crossed with *Bgn*$^{-/0}$ mice[1] and were then compared with their male littermates after 6 weeks of a Western-type diet. All animal care and experimental procedures were performed in accordance with the guidelines for the use of experimental animals as outlined in the *Deutsches Tierschutzgesetz* and were approved by the local Ethics Committee for animal experimentation *(Landesamt für Natur, Umwelt und Verbraucherschutz NRW).* Subcutaneously implanted Alzet® miniosmotic pumps (model 2004; mean pumping rate of 0,25 µl/h; Alzet Corporation, Cupertino, CA, USA) were used to provide treatment with the thrombin inhibitor argatroban (0.6 mg/kg/d; Mitsubishi Pharma Europe Ltd, London, United Kingdom) or respective vehicle (saline solution 0,9% with 300 mg/ml sorbitol and 400 mg/ml ethanol).

Isolation and semiquantification of biglycan from human and murine plasma

For analysis of circulating BGN, human plasma samples from patients without coronary heart disease (CHD), stable CHD and acute coronary syndrome (ACS) were collected at the *Klinik für Kardiologie, Pneumologie und Angiologie, Klinikum der Heinrich-Heine-Universität Düsseldorf,* Germany, with approval of the Human Ethics Commission of the Medical Faculty of the Heinrich-Heine Universität Düsseldorf (ethics vote 4739R) and informed consent of donors. Furthermore, plasma samples from C57BL/6J wildtype (WT) mice and *ApoE*$^{-/-}$ mice were analyzed.
Biglycan from plasma samples (murine samples were pooled from two animals each) was semipurified, digested with chondroitinase ABC (Seikagaku Corporation) to remove glycosaminoglycan chains, and subjected to polyacrylamide gel electrophoresis followed by Western blotting as previously described.[2] For validation of the assay, graded known amounts of intact biglycan (containing the protein core and glycosaminoglycan chains) were processed in parallel and under the same conditions.[2] The biglycan contents in samples were quantified after normalization to standard control.

Tissue processing

Mice were sacrificed at 15 or 30 weeks of age, respectively. For immunohistochemical staining of the aortic root, hearts were perfused with PBS, fixed in 4 % *p*-formaldehyde overnight, and either embedded in paraffin for 5 µm paraffin-sections or alternatively embedded in tissue-freezing medium (Tissue-Tek® O.C.T. Compound, Sakura® Finetek, Alphen aan den Rijn, Netherlands) for 14 µm cryosections.

Immunohistochemistry of the endothelial glycocalyx in cardiac tissue

Native hearts were cut in 10 (confocal images) or 20 µm cryosections. Slides were directly transferred to fixation buffer (70% MeOH, 5% acetic acid, 3.7% formalin in PBS), fixed for 20 minutes at 4℃, and then blocked for 1 h (10% FCS, 10% 10x TBS, 1% BSA in Aqua dest.). Polyclonal antiserum against murine biglycan (1:200, rabbit, LF159; kindly provided by Larry Fisher, National Institute of Dental and Cranofacial Research, National Institutes of Health, Bethesda, MD, USA) detected with a fluorophore-conjugated

secondary antibody (1:200, Alexa Fluor 647 goat-anti-rabbit IgG, Life Technologies GmbH, Darmstadt, Germany or anti- rabbit Alexa Fluor 568), Isolectin B4 Alexa Fluor 488 (1:1000, Invitrogen Life Technologies Corporation, Eugene, Oregon, USA) and anti-CD31 staining (1:20, abcam, Cambridge, UK), detected with secondary Rhodamine Red-X-conjugated antibody (1:100, Rhodamine Red-X-conjugated anti-rat IgG, Jackson Immunoresearch, West Grove, PA, USA) were used for analysis of vascular BGN deposition. Sections were mounted in Roti-Mount FluorCare DAPI (Carl Roth GmbH, Karlsruhe Germany). Representative pictures were taken at 630 fold magnification. For confirmation of BGN expression in the glycocalyx of cardiac capillaries Laser-scanning confocal microscopy was performed using a Zeiss LSM 510 META Laser Scanning Microscope.

Calibrated Automated Thrombography

Blood was collected from the retro-orbital plexus and anticoagulated with trisodium citrate (final concentration 0.38 %). Platelet free plasma (PFP) was generated by centrifuging twice for 10 minutes at 21 000 x g at room temperature. PFP was stored at -20℃ for later analysis.
Thrombin generation in murine plasma was measured by using Calibrated Automated Thrombography as described by Tchaikovski *et al.* with slight modifications[3, 4]. PPP-Reagent, Thrombin Calibrator and FluCa-Kit were purchased from Diagnostics Stago S.A.S (Asnières sur Seine, France). PPP-Reagent was diluted with PBS to reach a final concentration of 5 pM tissue factor in the assay. In some experiments alternatively negatively platelet membranes and recombinant human tissue factor (rhTF; Innovin®, Dade Behring, Germany) were used instead of PPP Reagent. Thrombin Calibrator was used in the same dilution as PPP- Reagent. Murine PFP was stimulated with dermatan sulfate (DS; Sigma Aldrich Chemie GmbH, Taufkirchen, Germany) or recombinant human biglycan (R&D Systems, Minneapolis, MN, USA) at a final concentration of 10 µg/ml or heparin (Enoxaparin; Clexane 40 mg/0,4ml, Sanofi Aventis, Frankfurt, Germany) at a final concentration of 3 µg/ml. For chondroitinase digestion, DS was preincubated with 2 mU/ml chondroitinase ABC (from *Proteus vulgaris;* Sigma Aldrich) for three hours at 37 ℃ prior to stimulat ion; for digestion with heparinase, DS or heparin were preincubated with 100 mU/ml heparinase (heparinase I/III blend from *Flavobacterium heparinum*; Sigma Aldrich) for 24 hours at 37 ℃ prior to sti mulation. Thrombin generation was measured in triplicates. 15 µl PFP were incubated with 25 µl diluted PPP-Reagent or diluted Thrombin Calibrator for 10 minutes at 33 ℃. The reaction was started by adding 20 µl FluCa buffer. The fluorescent signal was measured at 33℃ for 30 minutes using a Fluoroskan Ascent mi croplate reader (excitation: 390 nm, emission: 460 nm; Thermo Labsystems, Finland). Automatical data analysis was performed using Thrombinoscope™ Software.

Intravital microscopy of the carotid artery

Prior to the experiments, 8 x 10^6 platelets from donor mice were stained with 5-carboxyfluorescein diacetate succinimidyl ester (4.48 mM). *ApoE/Bgn*-double deficient mice were anesthetized with Ketamin (Ketavet®, Pfizer, 100 mg/kg) and Xylazin (2 % Bernburg, medistar, 5 mg/kg) by intraperitoneal (i.p.) injection. The common carotid artery was dissected free up to the bifurcation and the stained donor platelets were administered slowly intravenously. The interaction of the fluorescently labeled platelets and the vessel wall (rolling platelets) was visualized by intravital microscopy of the carotid artery near the bifurcation using a Leica microscope (20x water immersion objective, W20x/0,5; Leica DM2500MH). Rolling platelets were counted at three different positions near the bifurcation per mm^2.

Platelet activation

EDTA-anticoagulated blood was washed twice, and diluted 1:10 in Tyrode's buffer. Blood suspension was then incubated with fluorescein isothiocyanate–conjugated CD62P (P-selectin) monoclonal antibody (EMFRET Analytics, Eibelstadt, Germany). Samples were analysed using a Gallios Flow Cytometer (Beckman Coulter Inc.). Data analysis was performed with Kaluza Flow Analysis Software (Beckman Coulter Inc.).

Mass spectrometry of aortic extracellular matrix

Extracellular components of aortas from *ApoE*$^{-/-}$ mice and from *ApoE*$^{-/-}$/*Bgn*$^{-/0}$ mice were extracted and analyzed as previously described.[5,6] Briefly, after being harvested, each aorta was rinsed with ice-cold phosphate-buffered saline for removal of contamination with blood constituents. The ECM proteins of the aorta were solubilized in 4 M guanidinium chloride, 50 mM sodium acetate (pH 5.8) in the presence of proteinase inhibitors, and 25 mM ethylenediaminetetraacetic acid (EDTA) for 48 hours at room temperature. Data from mass spectrometric detection of proteins were expressed as spectral counts.

Flow cytometric analysis of aortic immune cell composition

Flow cytometric analysis of the aortas was performed as previously reported[7]. Briefly, for flow cytometric analysis, the aorta was dissected, and periaortic tissue was removed. The aortic wall was cut into small pieces and digested for 60 minutes at 37℃ in a solution of collagenase II (600 U/ml, Worthington Biochemical Corporation, Lakewood, USA) and DNase I (60U/ml, Roche Applied Science, Mannheim, Germany) as previously described.[8] To avoid unspecific binding isolated and suspended cells were incubated with Fc blocking agent (anti-mouse CD16/32 antibody, BioLegend, San Diego, CA, USA) before staining with the LIVE/DEAD Fixable Aqua Dead Cell Stain Kit (Invitrogen Life Technologies Corporation, Eugene, Oregon, USA) and the following antibodies: anti-CD3-APC/Cy7 (17A2), anti-CD11b-Pacific Blue™ (M1/70), anti-CD19-PacificBlue™ (6D5), anti-F4/80-Alexa Fluor® 488 (BM8), anti-Ly-6G-Pacific Blue™ (1A8) (all from BioLegend, San Diego, CA, USA), anti-CD45-PE (I3/2.3, Beckman Coulter Inc, Krefeld, Germany) and anti-CD11b-PE (M1/70, BD Biosciences, Franklin Lakes, NJ USA). Absolute cell concentrations were determined using Flow-Count™ Fluorospheres (Beckman Coulter Inc., Krefeld, Germany). Samples were measured on a Gallios™ Flow Cytometer (Beckman Coulter Inc., Krefeld, Germany). Data were analysed using Kaluza® Flow Analysis Software (Beckman Coulter Inc., Krefeld, Germany). Isotype control staining and fluorescence minus one (FMO)-staining were performed for each tissue. After exclusion of doublets, dead cells and cell debris, macrophages were detected in the CD45$^+$ leukocyte fraction by expression of CD11b and F4/80. Neutrophils were identified as CD11b$^+$/Ly-6G$^+$ cells. B and T cells were analyzed as CD19$^+$ (B cells) or CD3$^+$ (T cells) in the CD45$^+$ lymphocyte population. The amount of immune cells is expressed as number of cells per aorta.

(Immuno-)histochemistry

Histochemical and immunohistochemical (IHC) staining of the aortic root for the detection of macrophages and the analysis of plaque composition was performed as previously described.[7, 9] In detail, (immuno-)histochemical characterization of atherosclerotic lesions was performed in paraffin and frozen sections of the aortic root. Invasion of macrophages into atherosclerotic plaques was detected using an antibody against Mac-2 (1:1000, Cedarlane, Burlington, Canada) and a horseradish peroxidase (HRP)-conjugated secondary antibody (1:1500, goat-anti-rat IgG2a HRP, NB7126, novus biologicals, Littleton, CO, USA) and a monoclonal antibody against F4/80 (1:100, abcam, Cambridge, UK) and secondary HRP-conjugated antibody (1:200, goat-anti-rabbit IgG HRP, SantaCruz Biotechnologies, Dallas, TX, USA).

To investigate the fraction of smooth muscle cells (SMC) within the atherosclerotic lesion, paraffin sections were stained using a primary antibody against α-smooth muscle actin (1:300, abcam, Cambridge, UK) and a HRP-conjugated secondary antibody (1:400, goat-anti-rabbit IgG HRP, SantaCruz Biotechnologies, Dallas, TX, USA).

Immunohistochemical detection of the proteoglycans aggrecan, perlecan, and prolargin was performed in paraffin sections after previous antigen retrieval for 30 minutes with citrate buffer. Regarding the staining of aggrecan, perlecan, and versican pre-treatment with chondroitinase (chondroitinase ABC from *Proteus vulgaris*, Sigma-Aldrich Chemie GmbH, Steinheim, Germany) for one hour was used to expose the epitopes of the core proteins. Polyclonal antibodies were used to stain aggrecan (1:100, abcam, Cambridge, UK), prolargin(1:50, abcam, Cambridge, UK) and versican (1:200, abcam, Cambridge, UK). Detection was performed using HRP-conjugated secondary antibody (1:200, goat-anti-rabbit IgG HRP, SantaCruz Biotechnologies, Dallas, TX, USA). Perlecan was stained using a monoclonal antibody (1:25, Seikagaku, Tokyo, Japan) and HRP-conjugated secondary antibody (1:200, anti-goat-anti-rat IgG2a, novus biological, Littleton, CO, USA) in paraffin sections. Nuclei were detected using hematoxylin (Mayer's hemalum solution, Merck Millipore, Darmstadt, Germany). 3,3'-diaminobenzidine (DAB) (Zytomed, Berlin, Germany) was used as chromogen for detection.

To assess the proliferation index, 50 mg/kg of the antimetabolite 5-bromo-2'-deoxyuridine (BrdU, Sigma-Aldrich, St. Louis, MO, USA) were injected intraperitoneally (i.p.) 24 h and 1 h before sacrifice. Proliferating cells in atherosclerotic lesions were detected using primary antibody directed against incorporated BrdU (1:50, abcam, Cambridge, UK) and secondary antibody (1:200, Rhodamine Red-X-conjugated anti-rat IgG, Jackson Immuno Research, West Grove, PA, USA). Nuclei were counterstained using DAPI (Roti-Mount FluorCare DAPI, Carl Roth GmbH & Co. KG, Karlsruhe, Germany). Proliferation rate in lesions of the aortic root was expressed as BrdU positive cells per total nuclei.

Pictures were taken at 100 fold magnification. ImageJ software (ImageJ 1.37v software, NIH) was used to quantify positive stained area.

Cytokine and chemokine concentrations

Q-Plex Mouse Cytokine – Screen IR (Quansys Biosciences, Logan, UT, USA) was used to determine the concentrations of circulating chemokines and cytokines.

Analysis of circulating Heparin Cofactor (HC)II – thrombin complex

The amount of HCII/thrombin complex in EDTA-anticoagulated plasma of *ApoE*-KO and *ApoE/Bgn* DKO mice was determined using a HCII-thrombin mouse ELISA (CatNo. 27739, Bio-Medical, Peking, China) according to the manufacturer`s protocol.

Determination of atherosclerotic plaque burden of the aorta and the aortic root

At the indicated time points lipid staining (Oil Red O, Sigma-Aldrich Chemie GmbH, Steinheim, Germany) of the aorta and the aortic root was performed as described previously.[7]

Proteomic analysis of the aortic extracellular matrix

Aortic extracellular matrix proteins were extracted from mouse aortas using a three-step extraction method described previously.[5] Aortas from 15 week-old male *ApoE*-KO and *ApoE/Bgn* DKO mice were used for the experiment. In the *ApoE*-KO group (n=5), 5 pools of two aortas and in the DKO group (n=4), three pools of two aortas and one sample containing a single aorta were used. The aortas were cut into two halves, washed three times with ice-cold PBS containing 25 mM EDTA and 1% v/v protease inhibitors (P8340,

Sigma-Aldrich). In the first extraction step, the aortas were incubated with 0.5 M NaCl, 10 mM Tris-HCl, pH 7.5 supplemented with 25 mM EDTA and 1% v/v protease inhibitors (P8340, Sigma-Aldrich) with gentle shaking for 1 h at room temperature with a buffer to sample ratio of 10:1 (10 µl buffer per mg sample). In a second extraction step, the aortas were incubated in 0.08% SDS containing 25 mM EDTA and 1% v/v protease inhibitors (P8340, Sigma-Aldrich) for 2 h at room temperature with gentle shaking (10 µl buffer per mg sample). Finally, the aortas were extracted with 4 M guanidine hydrochloride, 50 mM sodium acetate, pH 5.8, 25 mM EDTA, 1% v/v protease inhibitors (P8340, Sigma-Aldrich). To facilitate the disruption of the extracellular matrix, the samples were vigorously vortexed for 72 h at room temperature (5 µl buffer per mg sample). For the proteomic analysis, the guanidine extracts were deglycosylated as described previously.[5] 25 µg proteins per sample were separated on a 4-12% Bis-Tris discontinuous polyacrylamide gradient gel (NuPAGE, Life Technologies). After silver staining, each lane was cut into 8 gel pieces which were subjected to in-gel tryptic digestion overnight on a robotic digestor (ProGest, DigiLab). Tryptic peptides were separated on a nano-flow HPLC system (RSLC 3000, PepMap100 C18 column, 25-cm length, 75-µm internal diameter, 3-µm particle size, Thermo Fisher Scientific) and eluted with a 40 min gradient (10-25% B in 35 min, 25-40% B in 5 min, 90% B for 10 min and 2% B for 20 min where A= 2% ACN, 0.1% formic acid in HPLC H2O and B = 80% ACN, 0.1% formic acid in HPLC H_2O). The eluted peptides were directly analyzed by a high mass accuracy tandem mass spectrometer (LTQ Orbitrap XL, Thermo Fisher Scientific) using full MS scan mode over the range of m/z 400-1600. MS/MS was performed on the 6 most abundant ions in each MS scan with dynamic exclusion. Raw files were searched against a mouse database (UniProt/Swiss-Prot 2012_03, 16520 entries) using Mascot 2.3.01 (Matrix sciences). Carboxyamidomethylation of cysteine was chosen as fixed modification and hydroxylation of lysine and proline as well as oxidation of methionine were selected as variable modifications. The mass tolerance was set at 10 ppm for the precursor ions and at 0.8 Da for fragment ions. Two missed cleavages were allowed. Scaffold (version 3.6.2, Proteome Software) was used to calculate the spectral counts and to validate MS/MS based peptide and protein identifications. The following peptide thresholds were applied: peptide probability > 95.0%, protein probability > 99.0% with at least 2 unique peptides.

Metabolic measurements and lipid profile

Analysis of body composition was determined by using the Minispec mq7.5 NMR analyzer (Bruker Corporation, Billerica, Massachusetts, USA). Lean mass and total body fat content were determined by nuclear magnetic resonance (NMR) spectroscopy (Bruker minispec, Bruker, Daltonik, Bremen, Germany) as previously described.[10]

Indirect calorimetry and physical activity were measured in a TSE cage system with a calorimetry module and infrared sensor frames. Animals were adapted to the cages 2-3 days before measurement. Parameters of indirect calorimetry and locomotor activity were measured for 72 h and analyzed over a period of 24 hours (CaloSys V2.1, ActiMot2, TSE Systems, Inc., Chesterfield, Missouri, USA) as described previously.[10]

The plasma concentrations of total circulating cholesterol, low densiy lipoprotein (LDL), very low density lipoprotein (VLDL), high-density lipoprotein (HDL) (Cholesterol Quantitation Kit, BioVision, Milpitas, CA, USA), and insulin (*Ultra Sensitive Rat Insulin ELISA* Kit, Chrystal Chem, Downers Grove, IL, USA) were determined.

Thrombosis measurement

The laser-injury induced thrombosis measurement in the carotid artery was performed as described previously[11, 12]. Briefly, an ultrasonic flow-probe (Transonic, Ithaca, NY, USA) was placed under the right common carotid artery below the bifurcation. The blood vessel was irradiated with a 540-nm green laser (Melles Griot Carlsbad, CA, USA) in direct proximity to

the flow probe. Endothelial injury and subsequent occlusive thrombus development were induced by injection of Rose Bengal (Acros Organics, Geel, Belgium) at a dose of 50 $mg \cdot kg^{-1}$ through a catheter placed in the left jugular vein. Determination of time to first and stable occlusion was conducted as previously defined[13].

Bleeding time

Mice were anesthetized and the tail was cut with a scalpel at a defined diameter. Bleeding time was assessed by measuring time from the incision to the cessation of bleeding[14].

Statistical analysis

Data are presented as mean ± SD unless otherwise stated. Normal distribution was assumed and parametric testing was performed. Statistical analyses were performed with GraphPad Prism software (La Jolla, CA, USA) using either one-way analysis of variance (ANOVA) with Dunnett's post hoc test or Student's *t*-test, as appropriate. Statistical significance was set at the level of $P<0.05$.

References

1. Tang T, Thompson JC, Wilson PG, Yoder MH, Mueller J, Fischer JW, Williams KJ, Tannock LR. Biglycan deficiency: Increased aortic aneurysm formation and lack of atheroprotection. *J Mol Cell Cardiol*. 2014;75:174-180
2. Moreth K, Brodbeck R, Babelova A, Gretz N, Spieker T, Zeng-Brouwers J, Pfeilschifter J, Young MF, Schaefer RM, Schaefer L. The proteoglycan biglycan regulates expression of the b cell chemoattractant cxcl13 and aggravates murine lupus nephritis. *J Clin Invest*. 2010;120:4251-4272
3. Tchaikovski SN, BJ VANV, Rosing J, Tans G. Development of a calibrated automated thrombography based thrombin generation test in mouse plasma. *J Thromb Haemost*. 2007;5:2079-2086
4. Hemker HC, Giesen P, Al Dieri R, Regnault V, de Smedt E, Wagenvoord R, Lecompte T, Beguin S. Calibrated automated thrombin generation measurement in clotting plasma. *Pathophysiol Haemost Thromb*. 2003;33:4-15
5. Didangelos A, Yin X, Mandal K, Baumert M, Jahangiri M, Mayr M. Proteomics characterization of extracellular space components in the human aorta. *Molecular & cellular proteomics : MCP*. 2010;9:2048-2062
6. Didangelos A, Yin X, Mandal K, Saje A, Smith A, Xu Q, Jahangiri M, Mayr M. Extracellular matrix composition and remodeling in human abdominal aortic aneurysms: A proteomics approach. *Molecular & cellular proteomics : MCP*. 2011;10:M111 008128
7. Grandoch M, Feldmann K, Gothert JR, Dick LS, Homann S, Klatt C, Bayer JK, Waldheim JN, Rabausch B, Nagy N, Oberhuber A, Deenen R, Kohrer K, Lehr S, Homey B, Pfeffer K, Fischer JW. Deficiency in lymphotoxin beta receptor protects from atherosclerosis in apoe-deficient mice. *Circ Res*. 2015;116:e57-68
8. Butcher MJ, Herre M, Ley K, Galkina E. Flow cytometry analysis of immune cells within murine aortas. *J Vis Exp*. 2011
9. Nagy N, Freudenberger T, Melchior-Becker A, Rock K, Ter Braak M, Jastrow H, Kinzig M, Lucke S, Suvorava T, Kojda G, Weber AA, Sorgel F, Levkau B, Ergun S, Fischer JW. Inhibition of hyaluronan synthesis accelerates murine atherosclerosis: Novel insights into the role of hyaluronan synthesis. *Circulation*. 2010;122:2313-2322
10. Fischer J, Koch L, Emmerling C, Vierkotten J, Peters T, Bruning JC, Ruther U. Inactivation of the fto gene protects from obesity. *Nature*. 2009;458:894-898
11. Wilson KM, Lynch CM, Faraci FM, Lentz SR. Effect of mechanical ventilation on carotid artery thrombosis induced by photochemical injury in mice. *Journal of thrombosis and haemostasis : JTH*. 2003;1:2669-2674
12. Freudenberger T, Deenen R, Kretschmer I, Zimmermann A, Seiler LF, Mayer P, Heim HK, Kohrer K, Fischer JW. Synthetic gestagens exert differential effects on arterial thrombosis and aortic gene expression in ovariectomized apolipoprotein e-deficient mice. *British journal of pharmacology*. 2014;171:5032-5048
13. Freudenberger T, Oppermann M, Heim HK, Mayer P, Kojda G, Schror K, Fischer JW. Proatherogenic effects of estradiol in a model of accelerated atherosclerosis in ovariectomized apoe-deficient mice. *Basic research in cardiology*. 2010;105:479-486
14. Fotinos A, Klier M, Gowert NS, Munzer P, Klatt C, Beck S, Borst O, Billuart P, Schaller M, Lang F, Gawaz M, Elvers M. Loss of oligophrenin1 leads to uncontrolled rho activation and increased thrombus formation in mice. *Journal of thrombosis and haemostasis : JTH*. 2015;13:619-630

Supplemental Figure I

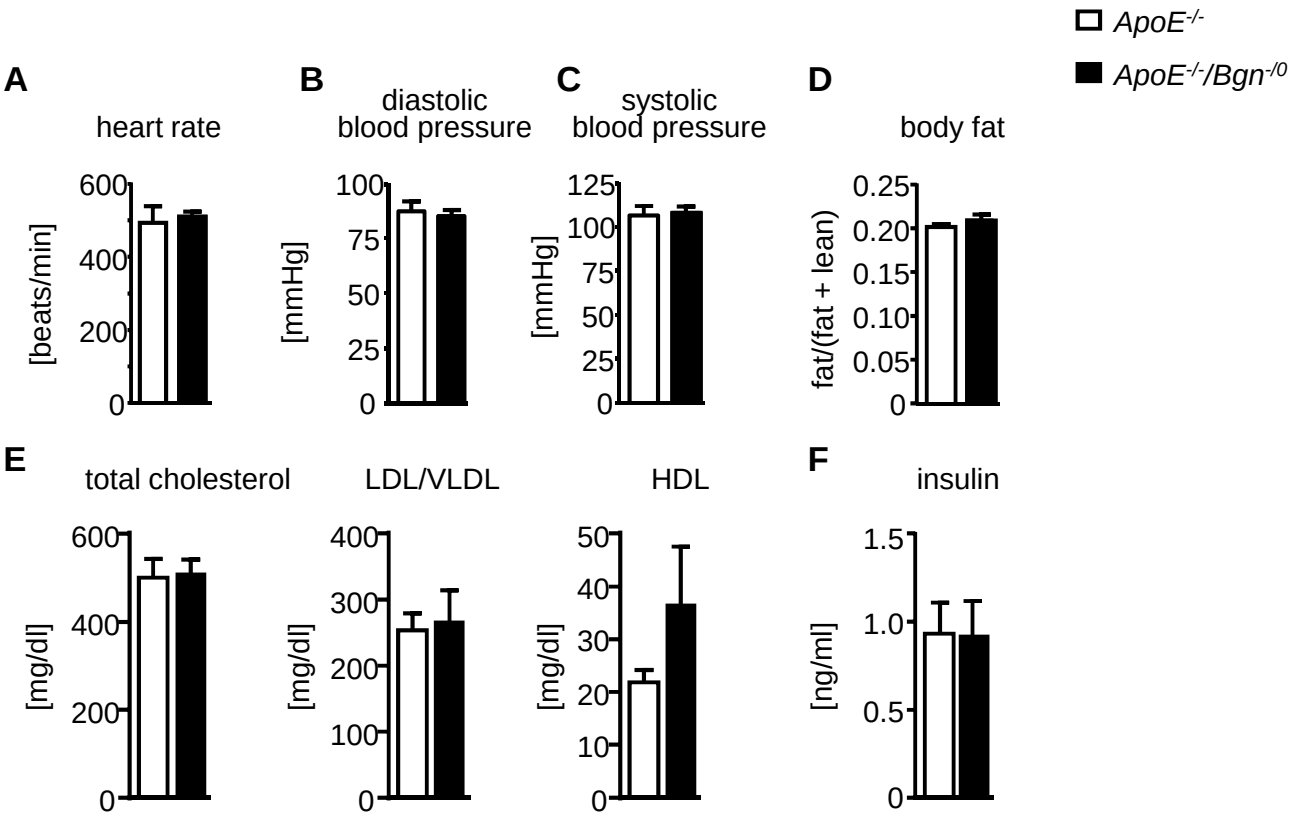

Supplemental Figure I

Characterization of basic cardiovascular and metabolic functions revealed no overt differences between the genotypes.

A, Heart rate**, B, C,** diastolic and systolic blood pressure of 15-week-old male *ApoE*- and *ApoE*/*Bgn*-deficient mice was determined by tail cuff plethysmography. n=4, 6. **D,** Total body fat mass relative to lean mass as determined by nuclear magnetic resonance (NMR) spectroscopy of 15-week-old male *ApoE*$^{-/-}$ mice and *ApoE*$^{-/-}$/*Bgn*$^{-/0}$ mice; n=8. **E,** Total cholesterol, low-density lipoprotein (LDL), very low density lipoprotein (VLDL), and high-density lipoprotein (HDL). **F,** Plasma concentrations of insulin in 15-week-old mice; n=8, 6. Data represent means ± SD.

Supplemental Figure II

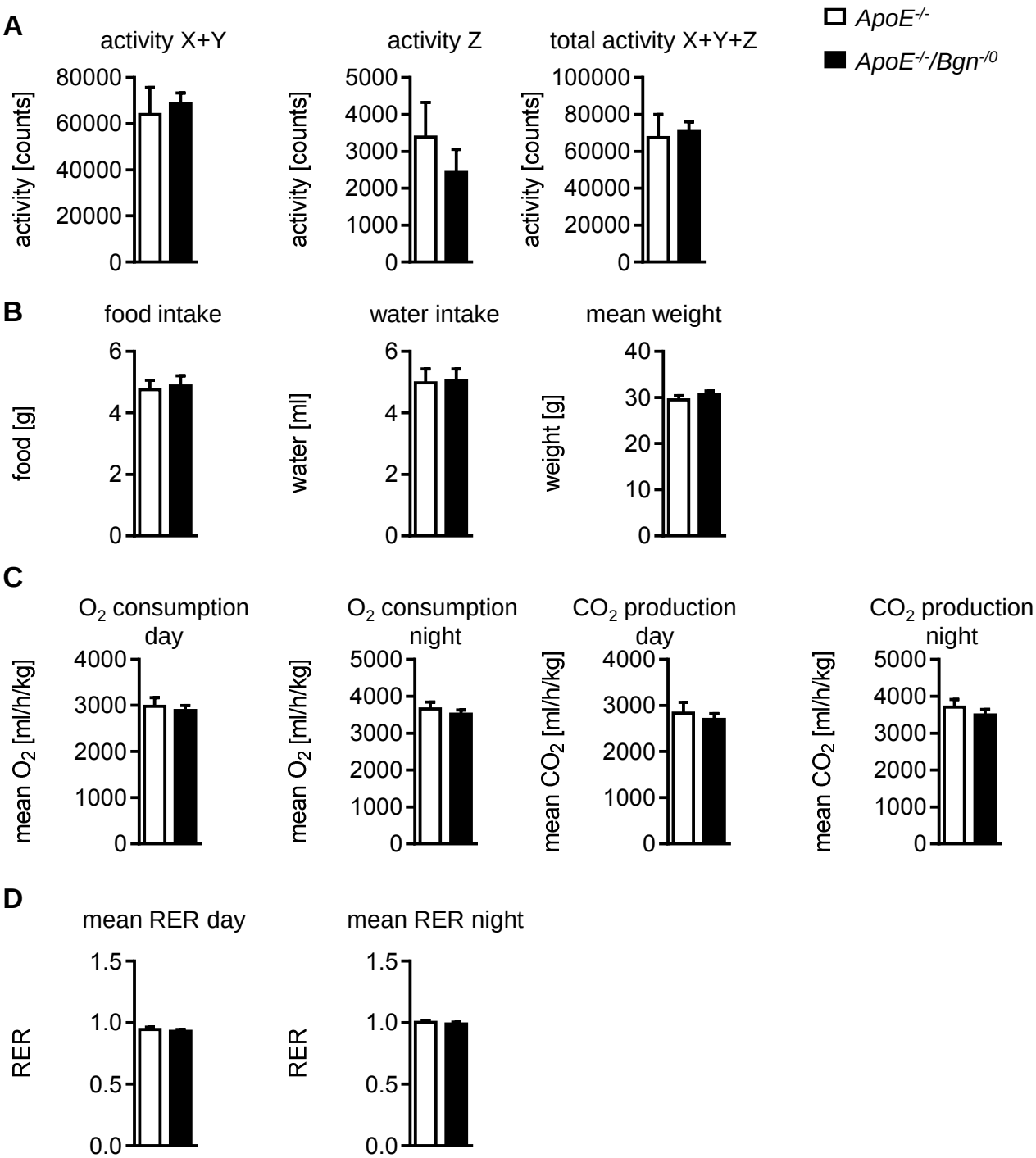

Supplemental Figure II

Basic physical activity, food and water intake and respiratory activity were not affected by the genetic deletion of *Bgn*.

A, Activity over X-, Y- and Z axis. **B,** Food, water intake, and weight. **C,** mean O2 consumption and CO_2 production at day and night. **D,** Respiratory exchange ratio (RER) as indicated in 15-week-old mice, n=8,6. Data represent means ± SD.

Supplemental Figure III

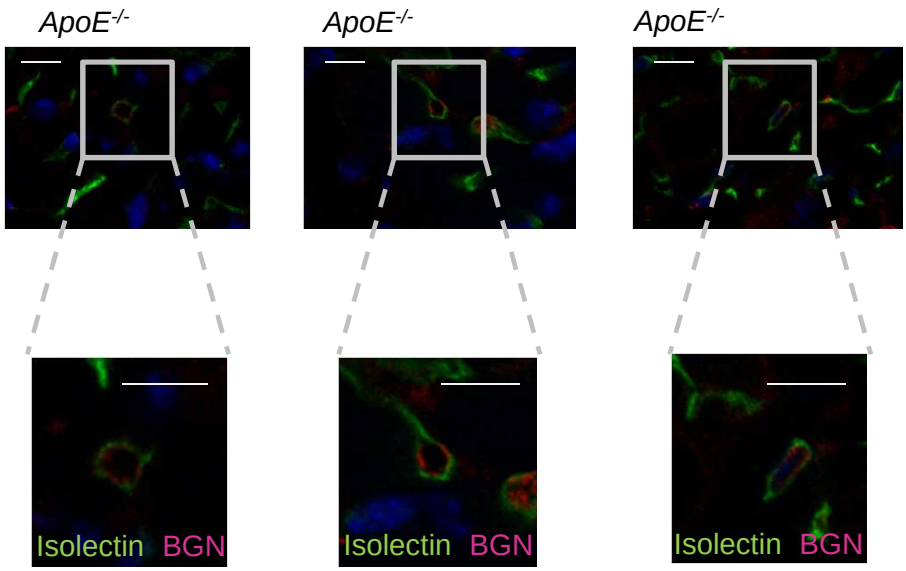

Supplemental Figure III

Bgn is localized in the glycolayx of cardiac capillaries.

Representative confocal images of BGN (red) and isolectin B4 (green) staining of small cardiac capillaries of *ApoE*-deficient mice. Nuclei are counterstained with DAPI. Scale bar represents 10 µm.

Supplemental Figure IV

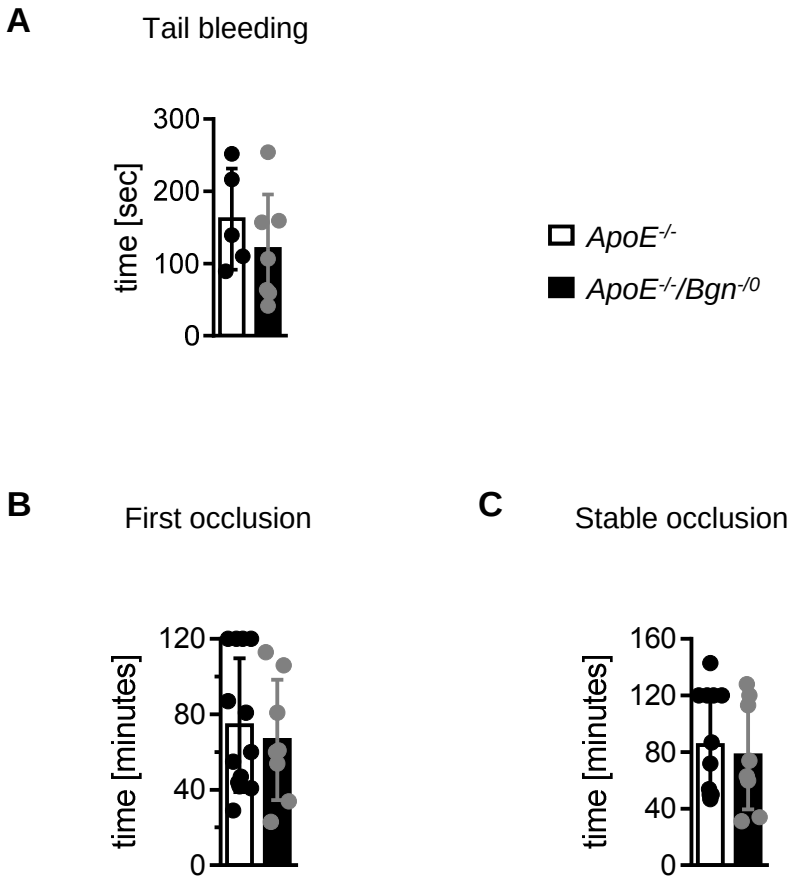

Supplemental Figure IV

Deficiency of *BGN* does not influence bleeding time and thrombus formation in *ApoE*-deficient mice

A, Tail bleeding assay was performed. Time to cessation of bleeding is shown, n=5,6. **B,C** Thrombosis measurement in *ApoE*- and *ApoE/Bgn*-deficient mice after laser-induced injury of the endothelium in the right common carotid artery. **B,** Time to first occlusion and **C,** stable occlusion are depicted; n=13,8. Data represent means ± SD.

Supplemental Figure V

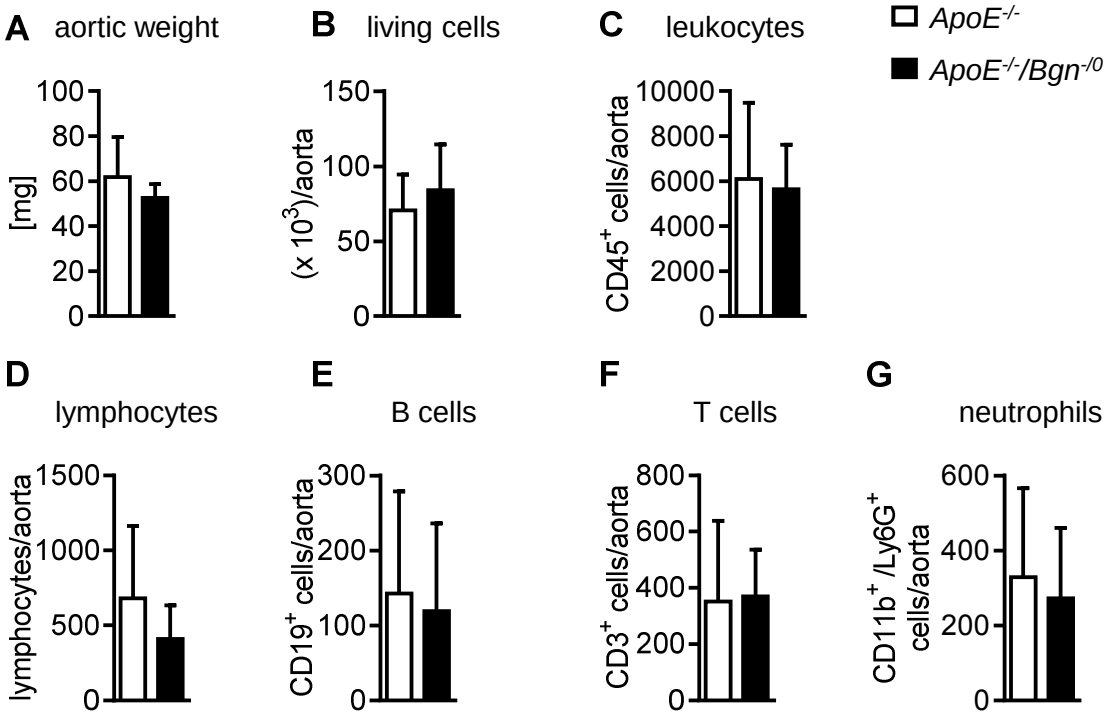

Supplemental Figure V

Flow cytometric analysis of immune cells in the aortic wall of *ApoE*$^{-/-}$ and *ApoE*$^{-/-}$*Bgn*$^{-/0}$ mice.

A, Aortic weight is shown. **B**, Numbers of living cells, **C,** $CD45^+$ leukocytes, **D,** lymphocytes, **E,** $CD45^+/CD19^+$ B cells, **F,** $CD45^+/CD3^+$ T cells, and **G,** $CD11b^+Ly6G^+$ neutrophils were analyzed. Absolute cell numbers per aorta are shown. n=11,8 (A-C), n=8,5 (D), n=6,4 (E,F), n=8,4 (G). Data represent means ± SD,

Supplemental Figure VI

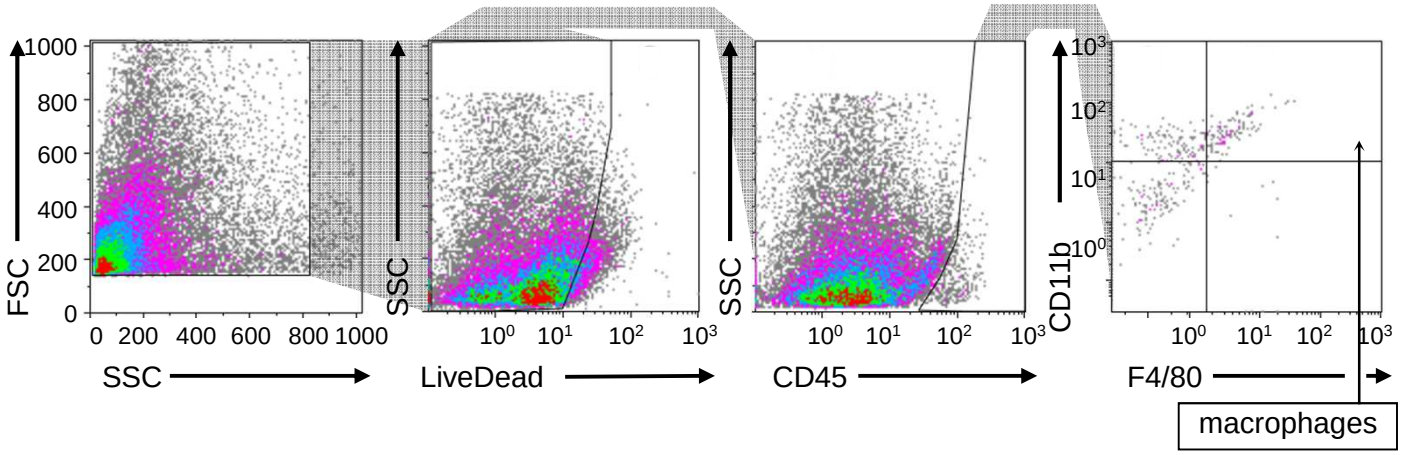

Supplemental Figure VI

Flow cytometric gating strategy for macrophage analysis.

Representative flow cytometric analysis of the aortic wall of 15-week-old *ApoE*$^{-/-}$ and *ApoE*$^{-/-}$/*Bgn*$^{-/0}$ mice. Macrophages (CD11b^{+}F4/80^{+} cells) were gated from living CD45^{+} leukocytes. FSC, forward scatter; SSC side scatter.

Supplemental Figure VII

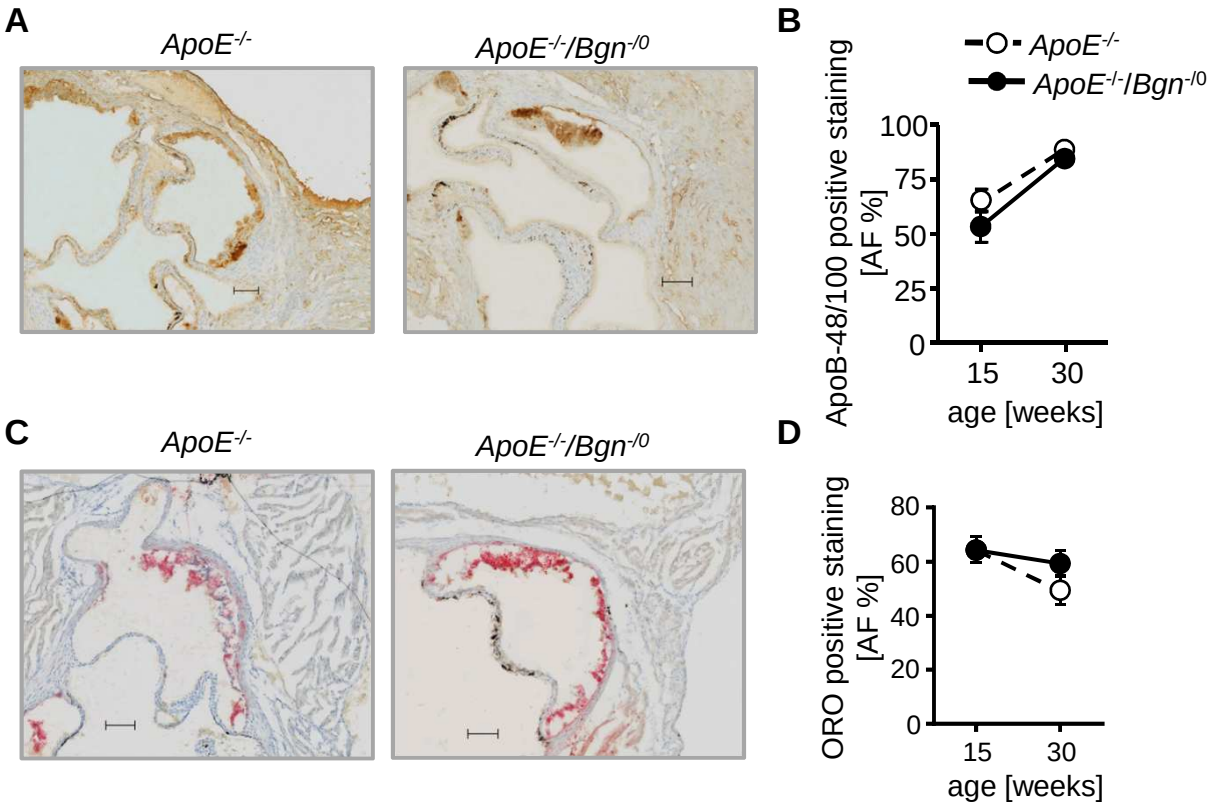

Supplemental Figure VII

Apolipoprotein B-48/100 expression and staining of total lipids.

A, Immunohistochemical analysis of aortic root plaques found no difference in apolipoprotein (Apo) B-48/100 deposition in aortic root plaques between *ApoE*$^{-/-}$*/Bgn*$^{-/0}$ and *ApoE*$^{-/-}$ mice. **B,** Quantitative analysis of ApoB-48/100; 15-week-old mice, n=3, 4; 30-week-old mice, n=10, 12. **C,** Staining of aortic root plaques from 15- and 30-week-old mice with Oil Red O found no differences in total lipid accumulation between the two genotypes at any time point as shown by quantitative analysis with ImageJ software; 15-week-old mice, n=15; 30-week-old mice, n=9, 12. Data represent means ± SD. Scale bar: 100 µm.

Supplemental Figure VIII

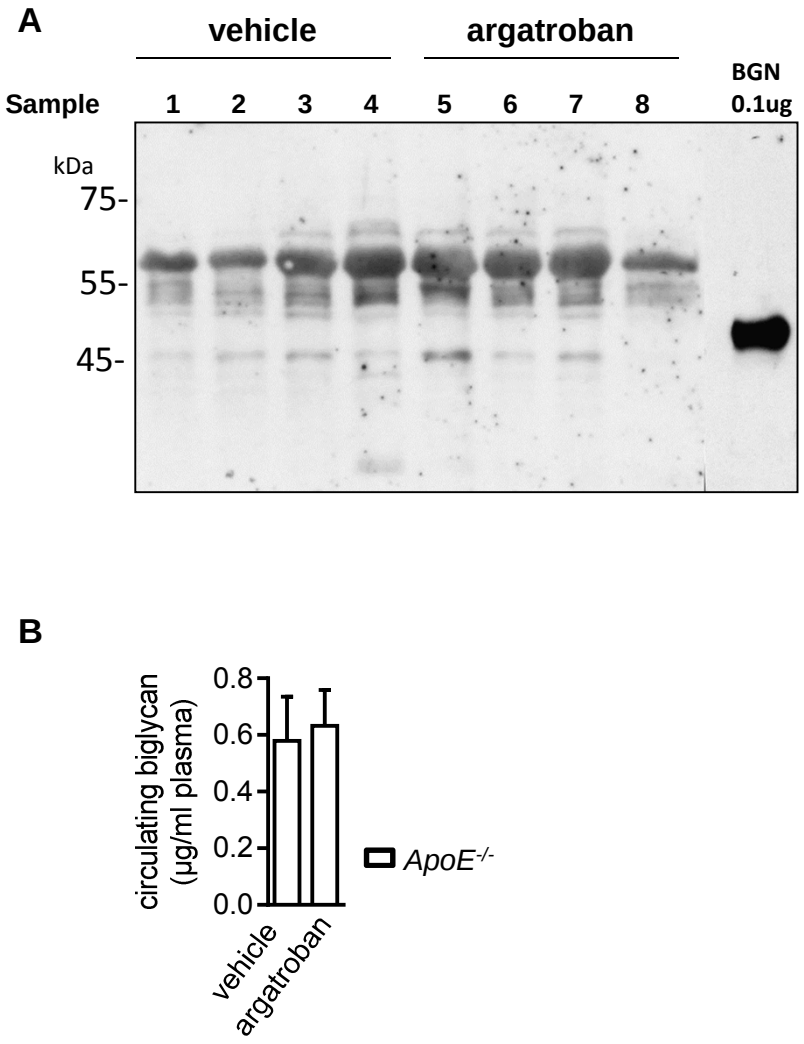

Supplemental Figure VIII

Circulating BGN in plasma of *ApoE*-deficient mice is not affected by treatment with argatroban.

A, Western blot analysis of circulating BGN core protein in plasma of male *ApoE*-deficient mice treated with argatroban or vehicle after chondroitinase ABC digestion. **B,** Quantification of biglycan content in plasma, n=4. Data represent means ± SD.

Supplemental Table I

	w/o CHD (n=7)	stable CHD (n=7)	NSTEMI (n=7)
age (years)	73.4 ± 2.2	74.7 ± 2.9	78.9 ± 2.8
sex (male/female)	5/2	5/2	5/2
BMI	26.4 ± 1.6	29.6 ± 1.4	28.5 ± 2.2
smoking	1/7	2/7	0/7
total cholesterol (mg/dl)	172.8 ± 21.5	137.2 ± 23.2	175.4 ± 24
diabetes mellitus	4/7	4/7	4/7
hypertension	4/7	6/7	4/7
prior MI	0/7	3/7	5/7
Hb	13.6 ± 1	12.2 ± 0.5	12.5 ± 0.9
WBC	8.1 ± 1.2	6.1 ± 0.8	7.1 ± 0.9
Hct (%)	40.4 ± 2.4	37.1 ± 1.2	36.9 ± 2.3
Plt	181.6 ± 12.3	242.4 ± 46.7	221.3 ± 13.6
ACEI/ARB	3/7	2/7	2/7
statins	4/7	3/7	4/7
heparin	1/7	0/7	0/7
ASA	2/7	5/7	6/7

Supplemental Table I

Baseline patient characteristics and medication. MI, myocardial infarction; Hb, hemoglobin; WBC, white blood cells; Hct, hematocrit; Plt, platelets; ACEI, angiotensin-converting-enzyme inhibitor, ARB, angiotensin II receptor blocker; ASA, acetylsalicylic acid

Supplemental Table II

Identified Proteins (65)	Accession Number	UniProt Name	MW (kDa)	Total Unique peptides	Total Unique spectra	Max % coverage	Total spectra	Average total spectra (*ApoE*$^{-/-}$)	Average total spectra (*ApoE*$^{-/-}$/*Bgn*$^{-/0}$)
Adiponectin	Q60994	ADIPO_MOUSE	27	31	33	15.8	90	9.6	10.5
Aggrecan core protein	Q61282	PGCA_MOUSE	222	27	29	3.8	43	1.4	9
Agrin	A2ASQ1	AGRIN_MOUSE	208	20	20	1.95	32	2.4	5
Alpha-1-antitrypsin 1-1	P07758	A1AT1_MOUSE	46	10	12	24.5	68	3.2	13
Alpha-1-antitrypsin 1-2	P22599	A1AT2_MOUSE	46	1	1	10.7	13	0	3.25
Alpha-1-antitrypsin 1-4	Q00897	A1AT4_MOUSE	46	13	13	23	97	9.2	12.75
Alpha-1-antitrypsin 1-5	Q00898	A1AT5_MOUSE	46	1	1	7.99	7	0	1.75
Apolipoprotein A-I	Q00623	APOA1_MOUSE	31	2	2	9.09	3	0.6	0
Apolipoprotein A-IV	P06728	APOA4_MOUSE	45	4	4	11.4	6	0	1.5
Asporin	Q99MQ4	ASPN_MOUSE	43	2	2	7.77	4	0.8	0
Basal cell adhesion molecule	Q9R069	BCAM_MOUSE	68	59	60	21.7	137	18	11.75
Basement membrane-specific heparan sulfate proteoglycan core protein	Q05793	PGBM_MOUSE	398	294	331	10.7	1080	118.2	122.25
Beta-2-glycoprotein 1	Q01339	APOH_MOUSE	39	76	93	37.7	148	17.6	15
Biglycan	P28653	PGS1_MOUSE	42	27	28	22.5	117	23.4	0
Cell surface glycoprotein MUC18	Q8R2Y2	MUC18_MOUSE	72	17	17	6.94	35	3.2	4.75
Chondroitin sulfate proteoglycan 4	Q8VHY0	CSPG4_MOUSE	252	3	3	1.68	5	0	1.25
Chymase	P21844	CMA1_MOUSE	28	2	3	10.9	4	0	1
Collagen alpha-1(I)	P11087	CO1A1_MOUSE	138	360	488	42	2218	233.4	262.75
Collagen alpha-1(II)	P28481	CO2A1_MOUSE	142	8	9	4.71	38	3.4	5.25
Collagen alpha-1(III)	P08121	CO3A1_MOUSE	139	255	303	37.8	843	87.4	101.5
Collagen alpha-1(IV)	P02463	CO4A1_MOUSE	161	6	6	1.74	9	1.8	0
Collagen alpha-1(VI)	Q04857	CO6A1_MOUSE	108	37	38	6.24	78	9	8.25
Collagen alpha-1(XV)	O35206	COFA1_MOUSE	140	8	8	2.12	11	1	1.5
Collagen alpha-1(XVIII)	P39061	COIA1_MOUSE	182	63	65	5.02	124	11	17.25
Collagen alpha-2(I)	Q01149	CO1A2_MOUSE	130	358	473	53.6	2277	233,8	277
Collagen alpha-2(IV)	P08122	CO4A2_MOUSE	167	11	11	2.58	15	1.8	1.5
Collagen alpha-2(VI)	Q02788	CO6A2_MOUSE	110	2	2	1.74	3	0	0.75
Connective tissue growth factor	P29268	CTGF_MOUSE	38	3	3	9.2	3	0	0.75
Decorin	P28654	PGS2_MOUSE	40	153	221	50	1045	108	126.25
Dermatopontin	Q9QZZ6	DERM_MOUSE	24	22	22	20.4	43	6	3.25
Elastin	P54320	ELN_MOUSE	72	2	2	3.72	2	0.4	0
EMILIN-1	Q99K41	EMIL1_MOUSE	108	4	4	2.06	4	0	1
Extracellular matrix protein 1	Q61508	ECM1_MOUSE	63	53	53	14.7	125	15.4	12
Extracellular superoxide dismutase [Cu-Zn]	O09164	SODE_MOUSE	27	70	105	41	363	44.2	35.5
Fibrillin-1	Q61554	FBN1_MOUSE	312	2	2	0.906	3	0	0.75
Fibronectin	P11276	FINC_MOUSE	273	427	555	23.3	3136	343	355.25
Galectin-1	P16045	LEG1_MOUSE	15	18	22	25.9	39	5.8	2.5
Hepatoma-derived growth factor	P51859	HDGF_MOUSE	26	22	24	31.6	35	4.4	3.25
Hepatoma-derived growth factor-related protein 3	Q9JMG7	HDGR3_MOUSE	22	8	8	11.9	11	2.2	0
Hyaluronan and proteoglycan link protein 1	Q9QUP5	HPLN1_MOUSE	40	2	2	6.18	3	0	0.75
Insulin-like growth factor-binding protein 7	Q61581	IBP7_MOUSE	29	84	111	55.5	188	17.6	25
Kininogen-1	O08677	KNG1_MOUSE	73	12	12	8.62	18	1.2	3
Laminin subunit alpha-2	Q60675	LAMA2_MOUSE	344	14	14	2.31	22	1.8	3.25
Laminin subunit alpha-4	P97927	LAMA4_MOUSE	202	18	18	3.52	26	3	2.75
Laminin subunit beta-1	P02469	LAMB1_MOUSE	197	18	18	3.47	29	2.6	4
Laminin subunit beta-2	Q61292	LAMB2_MOUSE	197	69	71	5.78	143	11.4	21.5
Laminin subunit gamma-1	P02468	LAMC1_MOUSE	177	68	69	9.83	135	10.8	20.25
Latent-transforming growth factor beta-binding protein 4	Q8K4G1	LTBP4_MOUSE	179	209	220	10.9	590	71.6	58
Leukocyte elastase inhibitor A	Q9D154	ILEUA_MOUSE	43	2	2	6.6	3	0	0.75
Lumican	P51885	LUM_MOUSE	38	59	73	16	291	32.6	32
Mast cell protease 4	P21812	MCPT4_MOUSE	27	36	39	37.8	60	5.2	8.5
Mimecan	Q62000	MIME_MOUSE	34	9	9	11.1	15	2.6	0.5
Neural cell adhesion molecule 1	P13595	NCAM1_MOUSE	119	31	34	8.34	50	4.6	6.75
Nidogen-1	P10493	NID1_MOUSE	137	19	19	3.94	32	3.2	4
Peptidase inhibitor 15	Q8BS03	PI15_MOUSE	29	10	10	11.6	17	3.4	0
Periostin	Q62009	POSTN_MOUSE	93	27	27	6.32	42	5.2	4
Prolargin	Q9JK53	PRELP_MOUSE	43	36	36	10.3	116	20	4
Prolow-density lipoprotein receptor-related protein 1	Q91ZX7	LRP1_MOUSE	505	4	4	0.594	5	1	0

Supplemental Table II

Extracted ECM proteins identified in isolated aortas from *ApoE*$^{-/-}$ and *ApoE*$^{-/-}$/*Bgn*$^{-/0}$ mice at 15 weeks of age. n=5,4 .

Supplemental Table III

Identified Proteins (65)	UniProt Name	MW (kDa)	Average normalised spectra *ApoE*$^{-/-}$	Average normalised spectra *ApoE*$^{-/-}$/*Bgn*$^{-/0}$	p-value (t-test)
Adiponectin	ADIPO_MOUSE	27	9.2 ± 3	10.7 ± 4.6	0.57
Aggrecan core protein	PGCA_MOUSE	222	1.2 ± 1.6	9.4 ± 4.8	0.0084
Agrin	AGRIN_MOUSE	208	2.3 ± 1.7	4.3 ± 1.5	0.097
Alpha-1-antitrypsin 1-1	A1AT1_MOUSE	46	2.9 ± 4	10.8 ± 3.2	0.015
Alpha-1-antitrypsin 1-2	A1AT2_MOUSE	46	0 ± 0	2.4 ± 4.8	0.29
Alpha-1-antitrypsin 1-4	A1AT4_MOUSE	46	8.3 ± 1.2	10.6 ± 3	0.16
Alpha-1-antitrypsin 1-5	A1AT5_MOUSE	46	0 ± 0	1.3 ± 2.6	0.29
Apolipoprotein A-I	APOA1_MOUSE	31	0.9 ± 1.9	0 ± 0	0.41
Apolipoprotein A-IV	APOA4_MOUSE	45	0 ± 0	1.2 ± 2.5	0.29
Asporin	ASPN_MOUSE	43	0.9 ± 1.9	0 ± 0	0.41
Basal cell adhesion molecule	BCAM_MOUSE	68	16.5 ± 2.5	10.2 ± 3.5	0.016
Basement membrane-specific heparan sulfate proteoglycan core protein	PGBM_MOUSE	398	128.9 ± 13.4	125.5 ± 18.6	0.76
Beta-2-glycoprotein 1	APOH_MOUSE	39	15.8 ± 1	12.6 ± 3.6	0.094
Biglycan	PGS1_MOUSE	42	23.6 ± 9.8	0 ± 0	0.0021
Cell surface glycoprotein MUC18	MUC18_MOUSE	72	3.5 ± 2.8	4.6 ± 3.1	0.57
Chondroitin sulfate proteoglycan 4	CSPG4_MOUSE	252	0 ± 0	1.2 ± 2.4	0.29
Chymase	CMA1_MOUSE	28	0 ± 0	0.7 ± 1.5	0.29
Collagen alpha-1(I)	CO1A1_MOUSE	138	245.6 ± 9.9	264.1 ± 59.8	0.51
Collagen alpha-1(II)	CO2A1_MOUSE	142	3.5 ± 3.6	5.6 ± 6.3	0.55
Collagen alpha-1(III)	CO3A1_MOUSE	139	104.6 ± 15.5	118.6 ± 31.6	0.41
Collagen alpha-1(IV)	CO4A1_MOUSE	161	1.5 ± 1.4	0 ± 0	0.068
Collagen alpha-1(VI)	CO6A1_MOUSE	108	11.7 ± 4.2	10.5 ± 1.5	0.61
Collagen alpha-1(XV)	COFA1_MOUSE	140	1.1 ± 1.5	1.5 ± 1.8	0.7
Collagen alpha-1(XVIII)	COIA1_MOUSE	182	10.2 ± 3.5	14.8 ± 2.3	0.061
Collagen alpha-2(I)	CO1A2_MOUSE	130	243.8 ± 17.7	272.6 ± 64.7	0.37
Collagen alpha-2(IV)	CO4A2_MOUSE	167	1.8 ± 1.7	1.7 ± 2.1	0.96
Collagen alpha-2(VI)	CO6A2_MOUSE	110	0 ± 0	0.9 ± 1.8	0.29
Connective tissue growth factor	CTGF_MOUSE	38	0 ± 0	0.6 ± 1.2	0.29
Decorin	PGS2_MOUSE	40	112.4 ± 12.4	124.7 ± 10.8	0.16
Dermatopontin	DERM_MOUSE	24	7.7 ± 3.6	4.4 ± 3.3	0.2
Elastin	ELN_MOUSE	72	0.6 ± 1.2	0 ± 0	0.41
EMILIN-1	EMIL1_MOUSE	108	0 ± 0	1 ± 1.2	0.11
Extracellular matrix protein 1	ECM1_MOUSE	63	14 ± 2.8	10.4 ± 2.3	0.081
Extracellular superoxide dismutase [Cu-Zn]	SODE_MOUSE	27	40.9 ± 6.1	29.7 ± 8.4	0.053
Fibrillin-1	FBN1_MOUSE	312	0 ± 0	0.7 ± 1.5	0.29
Fibronectin	FINC_MOUSE	273	332.9 ± 27.1	320.5 ± 29.8	0.53
Galectin-1	LEG1_MOUSE	15	7.5 ± 3.5	2.9 ± 3.5	0.091
Hepatoma-derived growth factor	HDGF_MOUSE	26	4.8 ± 1.8	3.6 ± 3	0.47
Hepatoma-derived growth factor-related protein 3	HDGR3_MOUSE	22	2 ± 1.3	0 ± 0	0.019
Hyaluronan and proteoglycan link protein 1	HPLN1_MOUSE	40	0 ± 0	0.7 ± 1.4	0.29
Insulin-like growth factor-binding protein 7	IBP7_MOUSE	29	16 ± 3	20.3 ± 4.6	0.14
Kininogen-1	KNG1_MOUSE	73	1.1 ± 1.6	2.5 ± 2.2	0.31
Laminin subunit alpha-2	LAMA2_MOUSE	344	2 ± 4.4	3.4 ± 4.3	0.63
Laminin subunit alpha-4	LAMA4_MOUSE	202	3.9 ± 2.5	3 ± 3.6	0.69
Laminin subunit beta-1	LAMB1_MOUSE	197	3.1 ± 4.4	4.1 ± 4.7	0.75
Laminin subunit beta-2	LAMB2_MOUSE	197	10.7 ± 5.6	18.2 ± 7.5	0.13
Laminin subunit gamma-1	LAMC1_MOUSE	177	13.5 ± 6.7	21.9 ± 8.1	0.13
Latent-transforming growth factor beta-binding protein 4	LTBP4_MOUSE	179	68.8 ± 5.9	51.6 ± 11.9	0.025
Leukocyte elastase inhibitor A	ILEUA_MOUSE	43	0 ± 0	0.7 ± 1.4	0.29
Lumican	LUM_MOUSE	38	31.6 ± 4.6	30 ± 4.2	0.61
Mast cell protease 4	MCPT4_MOUSE	27	4.8 ± 1.5	6.8 ± 1.6	0.094
Mimecan	MIME_MOUSE	34	3.2 ± 3.4	0.6 ± 1.2	0.19
Neural cell adhesion molecule 1	NCAM1_MOUSE	119	4.6 ± 4.9	5.9 ± 2.6	0.64
Nidogen-1	NID1_MOUSE	137	3.2 ± 2.6	3.1 ± 3.6	0.96
Peptidase inhibitor 15	PI15_MOUSE	29	3.1 ± 1.8	0 ± 0	0.013
Periostin	POSTN_MOUSE	93	7.5 ± 2	5.5 ± 1.7	0.14
Prolargin	PRELP_MOUSE	43	21.1 ± 8.2	4.7 ± 3.3	0.0072
Prolow-density lipoprotein receptor-related protein 1	LRP1_MOUSE	505	1.3 ± 1.9	0 ± 0	0.2
Sclerostin	SOST_MOUSE	23	3.3 ± 0.8	2 ± 1.4	0.12
Serine protease HTRA1	HTRA1_MOUSE	51	0.6 ± 1.2	0.7 ± 1.4	0.89
Serine protease inhibitor A3K	SPA3K_MOUSE	47	0 ± 0	0.7 ± 1.4	0.29
Serine protease inhibitor A3N	SPA3N_MOUSE	47	0 ± 0	1.2 ± 2.4	0.29
Serpin B6	SPB6_MOUSE	43	0 ± 0	0.7 ± 1.4	0.29
SPARC	SPRC_MOUSE	34	0 ± 0	1 ± 1.9	0.29
Versican core protein	CSPG2_MOUSE	367	2.3 ± 2.4	3 ± 2.4	0.68

Supplemental Table III

Differentially regulated extracted ECM proteins in isolated aortas from *ApoE*$^{-/-}$ and *ApoE*$^{-/-}$/*Bgn*$^{-/0}$ mice at 15 weeks of age. n= 5,4.